Unboundedness of the Hodge Local Euler Cocycle on Stellar Chains

Detailed definitions, the explicit periodic construction, and the bounded-homology obstruction

AI* not well verified exposition of the construction of N. Mnëv

September 2026

Abstract

For an oriented PL S^n–bundle, Mnëv's Hodge local Euler cocycle e_{CH} assigns a rational number to a chain of $n+1$ aggregations of oriented regular PL n–spherical cell complexes [13]. It is the Euler twisting cochain in a Hirsch–Brown homology model of the bundle. This exposition recalls the aggregation category, cellular Hodge contraction, and the precise formula for e_{CH}; then, for $n = 3$, it gives a fully explicit periodic chain of stellar subdivisions for which e_{CH} is logarithmically unbounded. The proof combines exact finite incidence calculations with a two-dimensional discrete elliptic argument on a periodic similarity-welded end.

A separate section explains the bounded-cohomology observation suggested by N. V. Ivanov. The universal Euler class of oriented PL S^3–bundles cannot have a bounded singular representative: this follows from Ivanov's vanishing theorem for bounded cohomology of simply connected spaces, or equivalently from the zero ℓ^1–seminorm of the fundamental class of S^4. We also spell out why this conceptual argument does not automatically imply unboundedness of a cocycle defined only on the nerve of the aggregation category; a norm-controlled comparison with singular bounded cohomology is needed. The explicit stellar construction proved here bypasses that issue.

*GPT-5.6 Sol

Contents

1 Purpose, context, and main statements

The subject is the size of a particular *local representative* of the Euler class, not merely the nontriviality of the Euler class itself. The relevant local representative is the Hodge-theoretic cocycle e_{CH} from [13]. For a chain of four subdivisions of triangulated 3–spheres it is obtained by alternating subdivision chain maps with the Moore–Penrose chain homotopies of the intermediate cellular chain complexes. The resulting scalar is a rational local formula for the Euler class.

The main result proved below is the following.

Theorem 1.1 (Main explicit theorem). *There is an explicit family of chains of four arrows*

$$K_0 \longrightarrow K_1 \longrightarrow K_2 \longrightarrow K_3(m) \longrightarrow K_4(m),$$

where every arrow is a composite of stellar subdivisions, such that

$$|e_{CH}(m)| \geq \frac{3\lambda}{40}\log m - O(1), \qquad \lambda = \frac{\log 5}{18\left(\log^2 5 + 4\arctan^2 2\right)} > 0.$$

Consequently

$$\sup |e_{CH}| = \infty$$

already on chains of iterated stellar subdivisions (equivalently, in the opposite direction, chains of stellar aggregations). Since the final number of tetrahedra is

$$f_3(K_4(m)) = 2m^2 + 42m + 48,$$

one also has

$$|e_{CH}(m)| \geq \frac{3\lambda}{80} \log f_3(K_4(m)) - O(1).$$

The proof of Theorem 1.1 is constructive. The special constant λ is not fitted numerically: it is forced by an exact 26–state seam problem and the zero-flux condition in the two widening lattice wedges. A first-order 32–state correction eliminates the only nonsummable discretization defect. The remaining global problem is handled on a protected middle range of radii. The correct scaling limit is not an ordinary Euclidean cone: the collapsed seam produces a similarity welding, which becomes a flat logarithmic cylinder in the symmetric sector. The complete finite certificates used in these two steps are recorded in Appendices B and C.

There is also a conceptual theorem, independent of the explicit construction.

Theorem 1.2 (Ivanov–Gromov obstruction, singular form). *Let $\mathscr{B}^+_{S^3}$ be a classifying space for oriented PL S^3–bundles, and let*

$$e_{PL} \in H^4(\mathscr{B}^+_{S^3}; \mathbb{R})$$

be its universal Euler class. Then e_{PL} is not represented by a bounded singular 4–cocycle. Equivalently,

$$e_{PL} \notin \operatorname{im}\big(H^4_b(\mathscr{B}^+_{S^3}; \mathbb{R}) \longrightarrow H^4(\mathscr{B}^+_{S^3}; \mathbb{R})\big).$$

The precise relation between Theorems 1.1 and 1.2 is discussed in Section 6. The second theorem alone does *not* automatically prove that a bounded function on simplices of an arbitrary category nerve is impossible; bounded cohomology is sensitive to the chain model and requires norm-controlled comparison maps. This distinction is important.

2 PL spherical cell complexes, subdivisions, and aggregations

2.1 Regular PL ball complexes

Definition 2.1 (Regular PL ball complex). A finite *regular PL ball complex* B on a compact polyhedron X is a finite collection of closed PL balls such that:

(i) the relative interiors of the balls form a partition of X;

(ii) the boundary of every ball is a union of balls of smaller dimension;

(iii) the intersection of two balls is a union of balls.

The face relation by inclusion gives a finite poset $P(B)$.

An *abstract* regular PL ball complex is the corresponding finite face poset, with the condition that the order complex of each principal ideal is a PL ball and the order complex of its proper part is its boundary sphere. In the spherical case the whole order complex is PL homeomorphic to a sphere. This is the language used in [12, 13].

Definition 2.2 (Oriented spherical complex). An oriented abstract regular PL n–spherical cell complex is such a complex S together with a choice of fundamental class

$$[S] \in H_n(S; \mathbb{Z}) \cong \mathbb{Z}.$$

For a chosen orientation of every n–cell, write

$$[S] = \sum_{\sigma \in S(n)} z_S(\sigma)\, \sigma, \qquad z_S(\sigma) \in \{\pm 1\}.$$

2.2 Subdivision and aggregation

Definition 2.3 (Geometric subdivision). Let B' and B be regular ball complexes on the same polyhedron X. We say that B' *subdivides* B if for every cell $b' \in B'$ there is a unique cell $b \in B$ such that

$$\operatorname{relint} b' \subset \operatorname{relint} b.$$

The resulting map $P(B') \to P(B)$ is the *aggregation map*; in the opposite direction one speaks of the subdivision.

An abstract aggregation is a map of abstract ball complexes which is geometrically realizable in this way, up to PL homeomorphism. Mnëv's category of combinatorial manifolds and aggregations is developed in [12]; its classifying space models the corresponding PL bundle classifying space. In [13] the oriented spherical version is the natural domain of the Euler local cocycle.

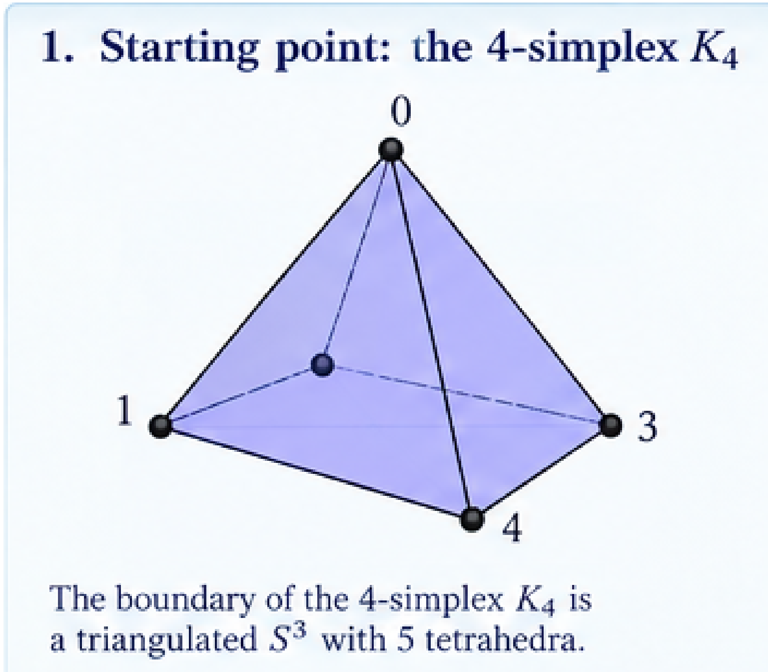

Figure 1: Schematic starting picture. The boundary $K_0 = \partial\Delta^4$ is a triangulated 3–sphere with five tetrahedral facets. The drawing is only a low-dimensional visual aid for the combinatorics of the boundary complex.

Definition 2.4 (Stellar subdivision)**.** Let K be a simplicial complex and let $F \in K$ be a simplex. Introduce a new vertex ν_F. The stellar subdivision at F replaces

$$\mathrm{st}_K(F) = F * \mathrm{lk}_K(F)$$

by

$$\nu_F * \partial F * \mathrm{lk}_K(F),$$

leaving the complement of $\mathrm{st}_K(F)$ unchanged. A finite composite of such moves is an *iterated stellar subdivision*; its inverse refinement arrow is an iterated stellar aggregation.

Stellar moves go back to Alexander [1]. We use only the subdivision direction in the explicit calculation because the induced chain maps then point in the same direction as the growing complexes. When the result is interpreted as a cocycle on the aggregation category, all arrows are reversed.

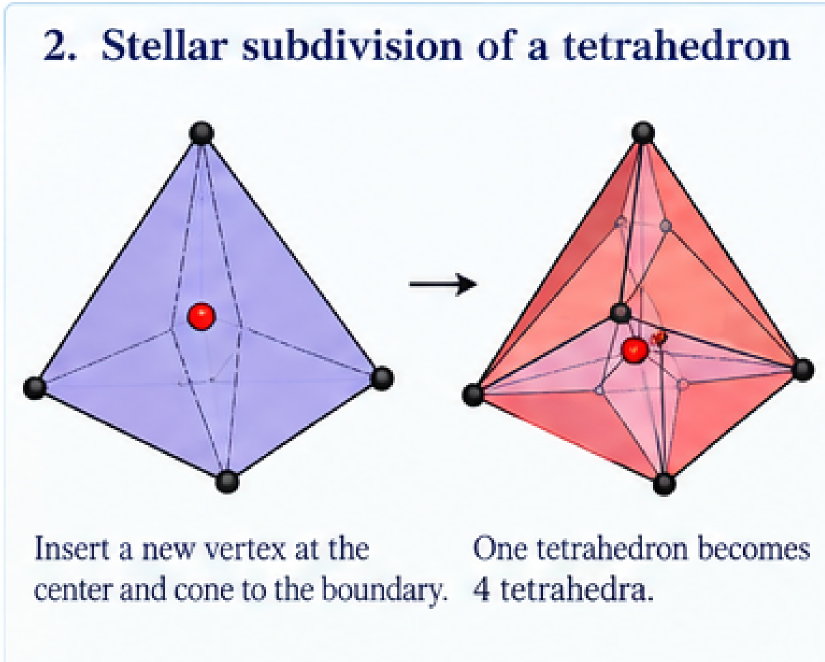

Figure 2: Stellar subdivision of a tetrahedron, shown schematically: insert a new interior vertex and cone it to the four boundary faces. One tetrahedron is thereby replaced by four tetrahedra.

2.3 The nerve and local cocycles

Let $\mathcal{S}_n^+$ denote the category whose objects are oriented abstract regular PL n–spherical cell complexes and whose morphisms are orientation-preserving aggregations. The nerve $N\mathcal{S}_n^+$ is the simplicial set with

$$(N\mathcal{S}_n^+)_k = \{S_0 \to S_1 \to \cdots \to S_k\}.$$

Thus an $(n+1)$–cochain on the nerve assigns a number to a chain of $n+1$ aggregation arrows, i.e. to $n+2$ spherical complexes. A local Euler formula is such a cochain representing the universal Euler class of oriented spherical PL bundles. The classifying-space viewpoint and the passage from local systems of aggregations to PL bundles are explained in [12, 13].

Definition 2.5 (Aggregation local system). Let B be a locally ordered simplicial complex. An oriented spherical aggregation local system on B is, equivalently, a simplicial map

$$B \longrightarrow N\mathcal{S}_n^+.$$

Thus every vertex v is assigned an oriented spherical complex S_v, every oriented edge v_0v_1 is assigned an aggregation $S_{v_0} \to S_{v_1}$, and the assignments commute on every 2–simplex (hence on all higher simplices). Such local systems are the combinatorial objects from which the associated PL spherical bundles are reconstructed in [12, 13].

3 Cellular Hodge contraction and the cocycle e_{CH}

3.1 Reminder: the Euler class as transgression

Let

$$S^n \longrightarrow E \xrightarrow{p} B$$

be an oriented spherical bundle. Orientation makes the local system $H^n(S^n;\mathbb{Z})$ trivial. In the cohomological Leray–Serre spectral sequence, if $u \in H^n(S^n;\mathbb{Z}) \cong \mathbb{Z}$ is the orientation generator, then

$$d_{n+1}(u) = e(p) \in H^{n+1}(B;\mathbb{Z}), \tag{1}$$

up to the standard global sign convention. Equivalently, cap product with $e(p)$ is the corresponding Gysin connecting homomorphism. The role of the Hirsch–Brown model is to realize the transgression (1) at chain level by a twisting cochain; e_{CH} is the combinatorial Hodge realization of its Euler component [2, 13].

3.2 Based cellular chains

Let S be a finite oriented regular PL n–spherical cell complex. Choose an orientation of every cell and let

$$C_q(S;\mathbb{Q})$$

be the cellular chain group with those oriented cells as an orthonormal basis. Write

$$\partial_q : C_q(S;\mathbb{Q}) \longrightarrow C_{q-1}(S;\mathbb{Q})$$

for the cellular boundary matrix and ∂_q^* for its transpose with respect to the standard Euclidean scalar products.

Definition 3.1 (Moore–Penrose inverse and Hodge homotopy). For a real or rational matrix A, its Moore–Penrose inverse $A^\dagger$ is the unique matrix satisfying

$$AA^\dagger A = A, \qquad A^\dagger A A^\dagger = A^\dagger, \qquad (AA^\dagger)^* = AA^\dagger, \qquad (A^\dagger A)^* = A^\dagger A.$$

For a cellular chain complex we put

$$h_q^S = (\partial_q^S)^\dagger : C_{q-1}(S;\mathbb{Q}) \to C_q(S;\mathbb{Q}).$$

The operator $h = \sum h_q$ is the canonical finite-dimensional Hodge chain contraction. In each degree it realizes the orthogonal splitting into boundaries, harmonic representatives, and coboundaries. In particular there are canonical projection/inclusion maps to homology for which

$$\partial h + h\partial = \mathrm{id} - ip.$$

For a sphere, only H_0 and H_n survive.

We use the normalized homology representatives

$$i_0^S(1) = \frac{1}{f_0(S)} \sum_{v \in S(0)} v \tag{2}$$

and

$$p_n^S(c) = \frac{1}{f_n(S)} \sum_{\sigma \in S(n)} z_S(\sigma) c(\sigma). \tag{3}$$

Thus p_n is the normalized coefficient of the fundamental class in coherent top-dimensional coordinates.

3.3 Subdivision chain maps

A subdivision $A : S \to S'$ induces a cellular subdivision chain map

$$A^{(q)} : C_q(S;\mathbb{Q}) \longrightarrow C_q(S';\mathbb{Q}),$$

obtained by replacing every old cell by the coherently oriented sum of its subcells. These maps commute with ∂ and send the fundamental class of S to the fundamental class of S'.

For a chain of $n+1$ subdivisions

$$S_0 \xrightarrow{A_0} S_1 \xrightarrow{A_1} \cdots \xrightarrow{A_n} S_{n+1},$$

the general Hodge expression is

$$e_{CH}(A_0, \ldots, A_n) = p_n^{S_{n+1}} A_n^{(n)} h_n^{S_n} A_{n-1}^{(n-1)} \cdots h_1^{S_1} A_0^{(0)} i_0^{S_0}(1). \tag{4}$$

For a chain of four subdivisions of oriented 3–spheres

$$S_0 \xrightarrow{A_0} S_1 \xrightarrow{A_1} S_2 \xrightarrow{A_2} S_3 \xrightarrow{A_3} S_4,$$

this becomes

$$e_{CH}(A_0, A_1, A_2, A_3) := p_3^{S_4} A_3^{(3)} h_3^{S_3} A_2^{(2)} h_2^{S_2} A_1^{(1)} h_1^{S_1} A_0^{(0)} i_0^{S_0}(1). \tag{5}$$

This is the $n = 3$ form of Mnëv's formula.

Theorem 3.2 (Mnëv's local Euler formula [13]). *For oriented PL S^n–bundles, the analogous matrix product with $n+1$ subdivision/aggregation arrows is an aggregation local combinatorial cocycle representing the rational Euler class. In the language of Hirsch–Brown models, it is the top component of the twisting cochain controlling the transgression differential in the Serre spectral sequence.*

The construction is conceptually close to Hirsch's homology model of a fibration and Brown's twisted tensor product; see [9, 2] and the discussion in [13].

3.4 Why the top Hodge step is an electrical network

For a triangulated oriented 3–sphere K, orient each tetrahedron by its increasing vertex order and write the fundamental cycle as

$$z = \sum_{\tau} z_\tau \tau, \qquad z_\tau \in \{\pm 1\}.$$

If tetrahedra τ, τ' share a triangle f, and $\epsilon_{\tau f}, \epsilon_{\tau' f} \in \{\pm 1\}$ are the corresponding boundary incidences, the identity $\partial z = 0$ gives

$$z_\tau \epsilon_{\tau f} + z_{\tau'} \epsilon_{\tau' f} = 0, \qquad z_\tau z_{\tau'} \epsilon_{\tau f} \epsilon_{\tau' f} = -1. \tag{6}$$

Thus, with $Z = \mathrm{diag}(z_\tau)$, $Z\partial_3^*\partial_3 Z$ has diagonal entries 4 and off-diagonal entry -1 precisely for dual-adjacent tetrahedra. It is exactly the ordinary unsigned dual graph Laplacian. This identity also shows that a global reversal of the fundamental orientation reverses the source and potential but cannot create or remove the logarithmic growth.

In coherent coordinates every triangle therefore lies in exactly two tetrahedra with opposite induced orientations. Consequently the top boundary matrix $D = \partial_3$ is, up to the coherent signs, the incidence matrix of the dual graph G_K whose vertices are tetrahedra and whose edges are triangles. Therefore

$$L = D^*D$$

is the ordinary graph Laplacian.

If $y \in C_2(K)$ and

$$p = L^\dagger D^* y,$$

then

$$Lp = D^*y, \qquad \sum_{v \in G_K} p(v) = 0.$$

Thus the last Hodge contraction is exactly the mean-zero Green potential of a finite electrical network. This observation is the bridge between the finite stellar calculation and the discrete harmonic analysis used below.

4 Proof architecture before the calculation

The explicit proof has six logically distinct steps.

1. Two initial stellar moves create the exact seed

$$x_2 = -\frac{1}{144}\big[(056) + (156) + (256) + (356)\big].$$

2. A three-move periodic stellar motif creates a long dual-graph horn with shells of size $4r + 7$ and cut size $4r + 26$.

3. The source in every stable shell has zero total charge, while the flux through every stable cut is $-1/18$.

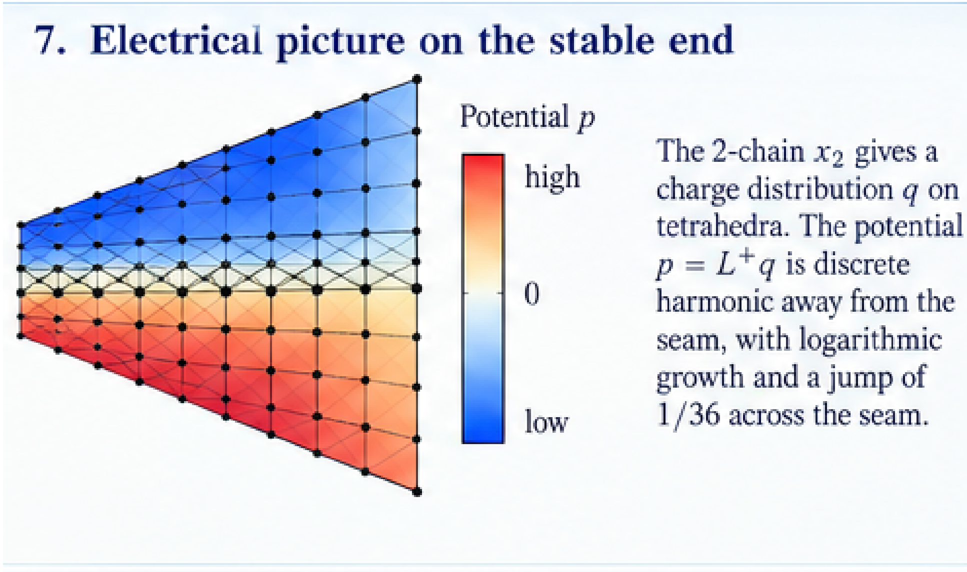

Figure 3: Electrical interpretation of the top Hodge step. In coherent top coordinates, $L_m p_m = q_m$ is a graph Poisson equation on the dual graph. The potential has a bounded transverse profile and a logarithmic radial component.

4. A fixed 26–state seam determines the boundary jump $V = 1/36$ of two widening square-lattice wedges. Zero longitudinal flux determines the positive logarithmic coefficient λ.

5. A finite 32–state first-order corrector makes the parametrix error summable. Zero-flux harmonic perturbations on the limiting cone have first nonconstant exponent

$$\alpha = \frac{\pi}{\arctan 2} > 2,$$

so arbitrary boundary data of size $O(m)$ disappears in a protected middle region.

6. The resulting oscillation $\gtrsim \log m$ is concentrated into the fourth arrow by repeated stellar subdivision of one maximizing tetrahedron.

The remainder of the proof is given in full detail in the next section.

5 The explicit periodic stellar family and proof

5.1 The family

Let

$$K_0 = \partial\Delta^4$$

with vertices $0, 1, 2, 3, 4$. For a based cellular complex K put

$$h_q^K = (\partial_q^K)^\dagger.$$

Let $i_0^K(1)$ be the normalized constant 0–cycle.

Perform first

$$K_0 \xrightarrow{A_0} K_1 = \mathrm{st}_{0123} K_0, \qquad K_1 \xrightarrow{A_1} K_2 = \mathrm{st}_{015} K_1,$$

and denote the new vertices by 5 and 6.

A direct exact calculation gives

$$x_2 := h_2^{K_2} A_1^{(1)} h_1^{K_1} A_0^{(0)} i_0^{K_0} = -\frac{1}{144}\big[(056) + (156) + (256) + (356)\big]. \tag{7}$$

Now put

$$T_0 = (5, 6, 3, 0).$$

If

$$T_j = (a_j, b_j, c_j, d_j),$$

perform

$$\mathrm{st}_{a_j b_j} \rightsquigarrow u_j, \qquad \mathrm{st}_{b_j c_j u_j} \rightsquigarrow v_j, \qquad \mathrm{st}_{d_j v_j} \rightsquigarrow w_j,$$

and set

$$T_{j+1} = (b_j, u_j, v_j, w_j).$$

After m repetitions let

$$A_2(m) : K_2 \longrightarrow K_3(m)$$

be the composite subdivision.

With the blocks numbered $j = 0, \ldots, m-1$, the first moving edge in block j has degree $j + 4$; the moving-edge fan induction in Appendix A

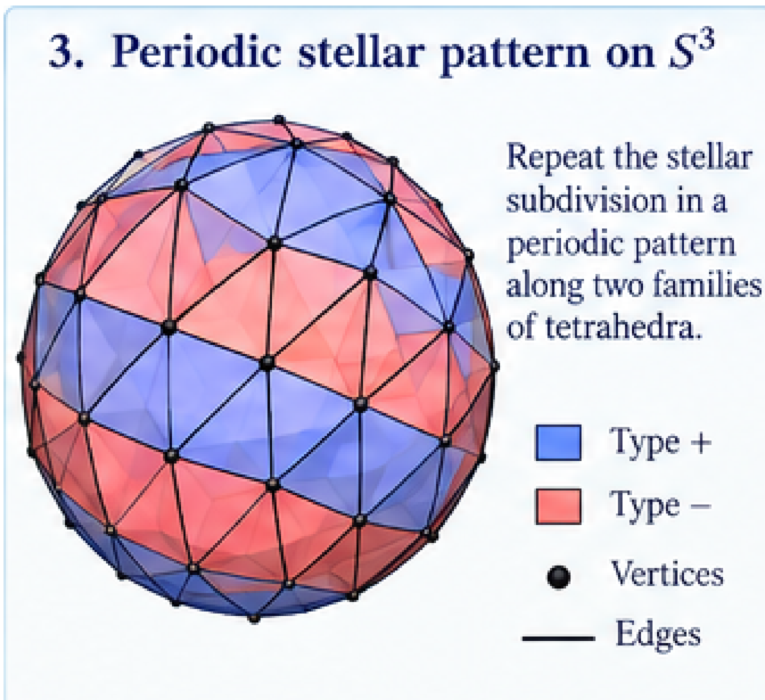

Figure 4: Schematic view of the periodic stellar motif on the 3–sphere. The actual construction is the three-move rule st_{ab}, st_{bcu}, st_{dv} written in the text; the colors indicate the two repeating sides of the growing region rather than additional structure.

gives this directly. The three stellar moves add respectively $j+4$, 4, and 3 tetrahedra. Hence

$$F_m := f_3(K_3(m)) = 12 + \sum_{j=0}^{m-1}(j+11) = 12 + 10m + \frac{m(m+1)}{2}. \qquad (8)$$

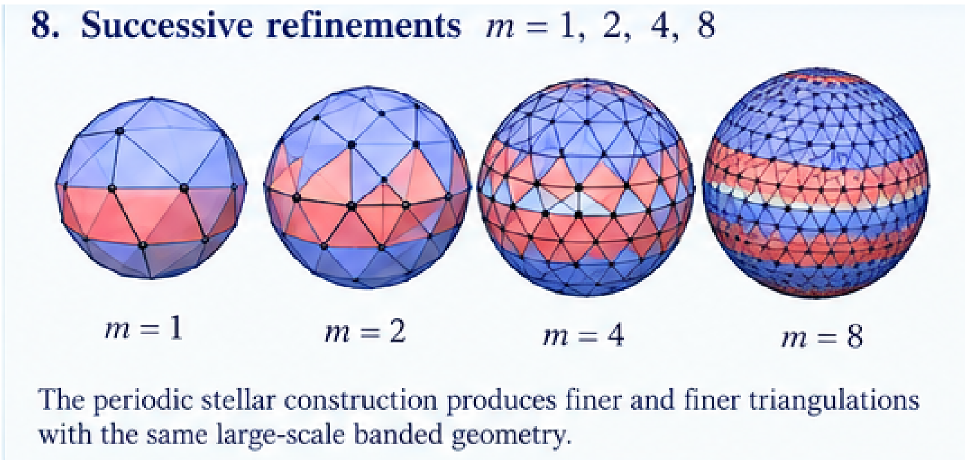

Figure 5: Schematic successive stages of the periodic stellar construction. Increasing m lengthens the stable periodic end while preserving its local motif and finite seam type.

Let z_m be the coherently oriented fundamental 3–cycle and put

$$x_m = h_3^{K_3(m)} A_2(m)^{(2)} x_2, \qquad p_m(\tau) = z_m(\tau) x_m(\tau).$$

In coherent coordinates the top Laplacian is the ordinary Laplacian L_m of the dual graph. Thus

$$L_m p_m = q_m, \qquad q_m = Z_m (\partial_3^{K_3(m)})^* A_2(m)^{(2)} x_2, \qquad (9)$$

and the Moore–Penrose normalization is

$$\sum_\tau p_m(\tau) = 0. \qquad (10)$$

5.2 The exact periodic end

Fix

$$\tau_* = (0, 9, 16, 22).$$

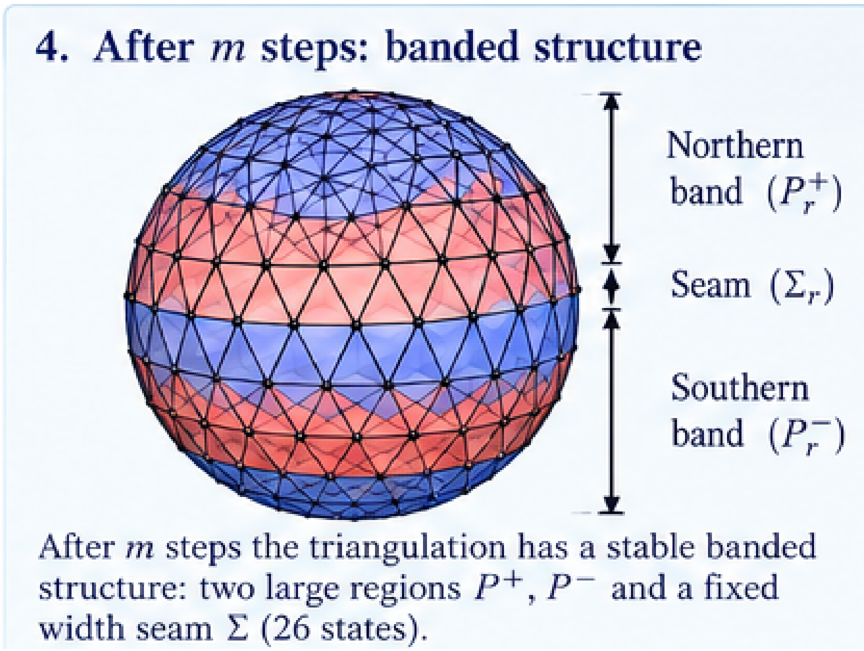

Figure 6: Large-scale schematic geometry after many motif repetitions. The periodic end consists of two widening regions joined along a fixed-width seam. The exact shell decomposition is $S_r = P_r^+ \sqcup P_r^- \sqcup \Sigma_r$.

For even m and
$$8 \le r \le \frac{m}{2} - 3,$$
let S_r be the distance-r shell about τ_* in the dual graph and let C_r be the set of dual edges from S_r to S_{r+1}.

Proposition 5.1 (all-radius stable combinatorics). *For every stable radius* $8 \le r \le m/2 - 3$ *one has*

$$S_r = P_r^+ \sqcup P_r^- \sqcup \Sigma_r, \tag{11}$$

where
$$|P_r^+| = 2r - 9, \qquad |P_r^-| = 2r - 10, \qquad |\Sigma_r| = 26.$$
The two $P_r^\pm$ *are source-free staircase paths. Their generic same-shell and radial incidence is the square-lattice incidence, with a fixed finite list of end corrections. The 26 seam states have an incidence pattern independent of* r *after the canonical shift of stellar labels. Consequently*

$$|S_r| = 4r + 7, \qquad |C_r| = 4r + 26. \tag{12}$$

Moreover

$$\sum_{\tau \in S_r} q_m(\tau) = 0, \qquad \sum_{\mathrm{dist}(\tau_*,\tau) \le r} q_m(\tau) = -\frac{1}{18}. \tag{13}$$

Proof. The closed formulas for every tetrahedron of P_r^+, P_r^- and Σ_r, together with all generic and exceptional radial adjacencies, are given in Appendix A. There the base shell S_8 is a finite face-adjacency check, and the induction $r \mapsto r+1$ is obtained by substituting the explicit stellar labels into the elementary stellar replacement rule. All four faces of every stable tetrahedron are accounted for, so the listed outward neighbors are exhaustive. This proves that the lists are the actual graph-distance shells, not merely abstract copies of the same local graph. Counting the displayed lists gives (12). The source is zero on the two paths and the seam table has six entries $+1/144$ and six entries $-1/144$; the finite base cumulative charge is $-8/144 = -1/18$, which then persists because every later stable shell has zero total charge. This proves (13). $\square$

The generic bulk incidence of Proposition 5.1 is the staircase approximation of the planar wedge

$$W = \{(x, y) : x > 0,\ 0 < y < 2x\}. \tag{14}$$

The decorated 26–vertex seam Σ_r and the twelve-wire source pattern are therefore genuinely periodic for every stable radius. Across a stable cut the chain $A_2(m)^{(2)}x_2$ is a twelve-wire flow: ten wires carry $-1/144$ and two carry $+1/144$ (with the global orientation convention used here).

Let L_Σ be the 26×26 Laplacian obtained from same-shell and radial seam-to-seam edges after identifying consecutive seams by the canonical shift. Let q_Σ be the corresponding 26–component source. The seam is connected, so

$$\ker L_\Sigma = \mathbb{R}1. \tag{15}$$

The equation

$$L_\Sigma U = q_\Sigma \tag{16}$$

has, modulo constants, the rational solution for which

$$144U_i \in \{0, 1, 2, 3, 4\}. \tag{17}$$

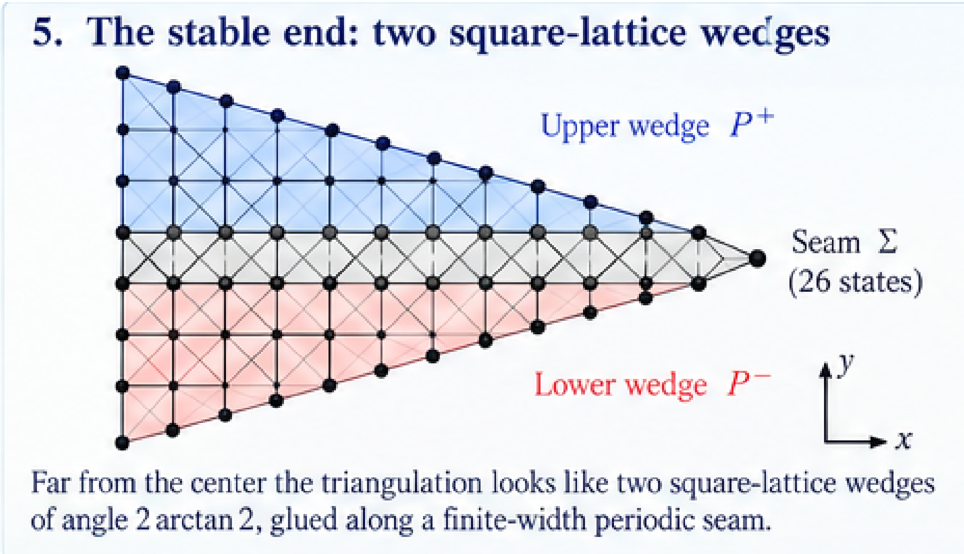

Figure 7: The stable end in flattened form: two staircase square-lattice wedges joined along a finite periodic seam. After rescaling, each side tends to the planar wedge $W = \{(x, y) : x > 0,\ 0 < y < 2x\}$.

The two endpoints of either growing wedge attach to seam states with values

$$0, \qquad V := \frac{1}{36}. \tag{18}$$

There is one further exact identity which is crucial. Orient radial seam edges from S_r to S_{r+1}. Then

$$J_\Sigma := \sum_{(i,j)\in E_\Sigma^+} (u_i - u_j) = -\frac{1}{18}. \tag{19}$$

Thus the leading seam cell already carries the entire through-current in (13).

The persistence of this finite cell for every stable radius is proved from closed stellar-label formulas in Appendix A. The complete 26–state incidence table, including the source values, the rational cell solution, radial degrees, path attachments, and incoming and outgoing seam states, is reproduced in Appendix B. It is an exact finite certificate for (16)–(19).

5.3 The logarithmic coefficient

Put

$$L = \log 5, \qquad \theta_0 = \arctan 2.$$

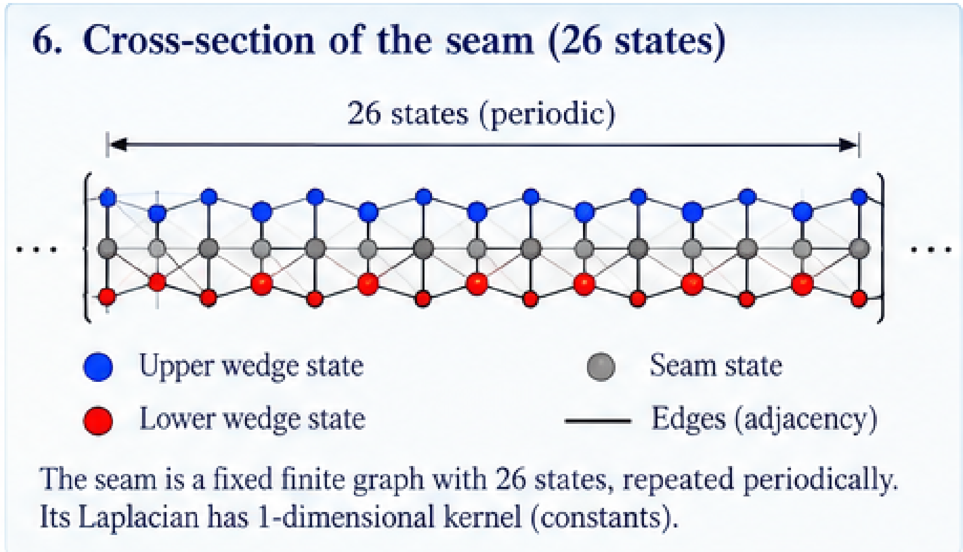

Figure 8: Schematic cross-section of the fixed periodic seam. The rigorous calculation uses the exact 26–state incidence table and its graph Laplacian L_Σ; this drawing is intended only to visualize a finite scattering cell repeated from shell to shell.

The continuum scaling profile in either growing wedge has the form

$$P^{(0)}(r,t) = \lambda \log r + F(t), \qquad F(t) = \frac{\lambda}{2}\log(1+t^2) + B\arctan t, \quad 0 \le t \le 2. \tag{20}$$

Here r is the longitudinal lattice coordinate and t is the quotient of transverse and longitudinal coordinates.

Lemma 5.2. *For the periodic stellar end the logarithmic coefficient is*

$$\lambda = \frac{\log 5}{18\left(\log^2 5 + 4\arctan^2 2\right)} > 0. \tag{21}$$

Proof. By (18), the two side values of one widening wedge differ by $V = 1/36$. Hence

$$\frac{\lambda L}{2} + B\theta_0 = V. \tag{22}$$

By (19), the leading seam cell carries the whole through-current $-1/18$ of (13). Hence the sum of the two leading wedge currents is zero. The two leading continuum boundary problems are mirror copies: the attachment values are $0, V$ on one path and $V, 0$ on the other, with the transverse coordinate reversed on P_r^-. Their longitudinal currents are therefore equal, so each widening wedge has zero leading longitudinal flux. Since

$$\partial_r P^{(0)}(r,t) = \frac{1}{r}\left(\lambda - tF'(t)\right),$$

the continuum flux across a longitudinal section is

$$\int_0^2 \frac{\lambda - Bt}{1+t^2}\,dt = \lambda\theta_0 - \frac{B}{2}L.$$

Thus

$$\lambda\theta_0 - \frac{B}{2}L = 0. \tag{23}$$

Solving (22) and (23), and using $V = 1/36$, gives (21). □

Numerically,

$$\lambda = 0.011932257088851988\ldots.$$

5.4 A first-order discrete parametrix

We now make the first discrete correction completely finite. Order the two bulk paths as

$$P_r^+ = (v_0^+, \ldots, v_{2r-10}^+), \qquad P_r^- = (v_0^-, \ldots, v_{2r-11}^-).$$

With the state numbering of the 26–state seam table, the same-shell attachments are

$$s_1 \sim v_0^+, \qquad s_3 \sim v_{2r-10}^+, \qquad s_{10} \sim v_0^-, \qquad s_{11} \sim v_{2r-11}^-,$$

and the corresponding values of U are $0, V, V, 0$.

Sample the continuum profile by

$$P_0(s_i) = \lambda \log r + U_i, \tag{24}$$
$$P_0(v_k^+) = \lambda \log r + F(k/r), \tag{25}$$
$$P_0(v_k^-) = \lambda \log r + F(2 - k/r). \tag{26}$$

The harmless bounded shifts hidden in the staircase embedding have merely been fixed by this choice of coordinates; changing them changes only the first corrector below.

Define the enlarged first-order cell

$$\widehat{\Sigma}_r = \Sigma_r \cup \{v_0^+, v_{2r-11}^+, v_{2r-10}^+, v_0^-, v_1^-, v_{2r-11}^-\}. \tag{27}$$

The six additional states are precisely the path states at which the coefficient of r^{-1} in $LP_0 - q$ can be nonzero. Identifying consecutive shells by the seam shift and by distance from the appropriate path end turns (27) into a fixed 32–state graph. Let $\widehat{L}$ denote its integer graph Laplacian, counting both same-shell and radial edges which survive at order r^{-1}.

Lemma 5.3 (exact 32–state corrector). *The graph underlying $\widehat{L}$ is connected, and therefore*

$$\ker \widehat{L} = \mathbb{R}1. \tag{28}$$

As an independent integer certificate, deleting the last row and column of the state ordering used above gives the nonzero principal cofactor

$$\det \widehat{L}^{(32)} = 71\,987\,392. \tag{29}$$

The full state ordering, quotient edge list, the first-order defect vector a, and its exact compatibility identity are given in Appendix C.

For the function P_0 of (24)–(26) there is a fixed vector $a \in \mathbb{R}^{32}$ such that on the states of $\widehat{\Sigma}_r$

$$LP_0 - q = \frac{a}{r} + O(r^{-2}), \tag{30}$$

and

$$\langle a, 1 \rangle = 0. \tag{31}$$

Outside $\widehat{\Sigma}_r$ the total ℓ^1–norm of the defect on one shell is $O(r^{-2})$. Consequently the finite equation

$$\widehat{L}W = -a, \qquad \langle W, 1 \rangle = 0, \tag{32}$$

has a unique solution.

Proof. Everything is a local incidence calculation. The 26 seam states are periodic under the canonical shift. On P_r^+ only the positions $0, 2r-11, 2r-10$ can fail to have the ordinary square-lattice stencil at first order; on P_r^- the corresponding positions are $0, 1, 2r-11$. The quotient on these $26+6$ states has 32 vertices. It is connected without any determinant calculation: the 26 seam states form a connected graph; ν_0^+ attaches to s_1; the two upper-end P^+ states attach to s_3, s_4, s_6; ν_0^-, ν_1^- attach to $s_4, s_{10}, s_{14}, s_{17}$; and the remaining lower-end P^- state attaches to s_{11}. Hence the kernel of its graph Laplacian consists of constants. Direct integer elimination gives the optional cofactor certificate (29).

The expansion uses only

$$\log(r \pm 1) = \log r \pm r^{-1} + O(r^{-2}),$$

$$F(t) = F(0) + F'(0)t + O(t^2), \qquad F(2-t) = F(2) - F'(2)t + O(t^2),$$

with

$$F'(0) = B, \qquad F'(2) = \frac{2\lambda + B}{5}.$$

The constant term is exactly the 26–state equation (16), together with the four attachment values $0, V, V, 0$. The coefficient of r^{-1} is therefore supported on $\widehat{\Sigma}_r$ and is independent of r after identification. Direct addition of the 32 entries gives zero identically, separately in the coefficients of B and λ. Equivalently, summing the discrete Laplacian over the whole shell leaves the difference of consecutive cut fluxes; the leading cut flux is constant, so no r^{-1} shell charge can occur. This proves (31). Finally (28) and (31) give (32). $\square$

Lemma 5.4 (summable parametrix). *There is a function P on the infinite stable periodic end such that, for all sufficiently large shells,*

$$\sum_{\nu \in S_r} |LP(\nu) - q(\nu)| \le Cr^{-2}, \tag{33}$$

$$\Phi_P(r) = -\frac{1}{18} + O(r^{-1}), \tag{34}$$

and, for every fixed seam state σ_r transported by the canonical shift,

$$P(\sigma_{2r}) - P(\sigma_r) = \lambda \log 2 + O(r^{-1}). \tag{35}$$

Proof. Let W be the solution of (32). Put W_ν/r on the 32 states of $\widehat{\Sigma}_r$. On the regular part of P_r^+ interpolate, as a fixed smooth function of $t = k/r$, between the values of W at the two interface states ν_0^+ and ν_{2r-11}^+. On the regular part of P_r^- interpolate similarly between ν_1^- and ν_{2r-11}^-. Multiply both interpolants by r^{-1} and call the resulting global correction R.

At the 32 first-order states the coefficient of r^{-1} in LR is exactly $\widehat{L}W = -a$, so (30) is cancelled. On the regular wedge vertices R is a smooth homogeneous expression of degree -1; hence its second derivatives are $O(r^{-3})$. Since a shell contains $O(r)$ regular wedge vertices, their total contribution is $O(r^{-2})$. The sampled harmonic profile P_0 has the usual five-point residual $O(r^{-4})$ away from the fixed boundary layer, and the remaining finitely many second-order boundary-layer errors are $O(r^{-2})$. Therefore $P = P_0 + R$ satisfies (33).

For the flux no summation from infinity is needed. The sampled seam profile has leading radial flux $-1/18$ by (19), while the two sampled continuum wedges have zero leading longitudinal flux by (23). Their discretization error changes the cut flux by $O(r^{-1})$. The correction R has size $O(r^{-1})$. On the $O(r)$ generic cut edges its radial differences are $O(r^{-2})$; on the finitely many interface edges they may be $O(r^{-1})$. Both contributions to the cut flux are therefore $O(r^{-1})$. This proves (34) directly. Finally on a shifted seam state

$$P(\sigma_r) = \lambda \log r + U_\sigma + \frac{W_\sigma}{r} + O(r^{-2}),$$

which gives (35). $\square$

5.5 Zero-flux decay on the similarity-welded stable end

For a function h on a shell put

$$\omega_h(r) = \max_{S_r} h - \min_{S_r} h.$$

For $v \in S_r$ let $d_+(v)$ and $d_-(v)$ be the numbers of neighbors in S_{r+1} and S_{r-1}. The all-radius incidence table of Appendix A gives

$$\sum_{S_r} d_+ = 4r + 26, \qquad \sum_{S_r} d_- = 4r + 22,$$

and only fifteen vertices have $d_+ \neq d_-$. Define

$$A_r(h) = \frac{1}{4r+26} \sum_{S_r} d_+(v)h(v), \qquad B_r(h) = \frac{1}{4r+22} \sum_{S_r} d_-(v)h(v).$$

The exact fifteen-state identity gives

$$|A_r(h) - B_r(h)| \leq \frac{C}{r}\, \omega_h(r). \tag{36}$$

If h is harmonic on an annulus and $\Phi(h)$ is its constant outward flux, exact Gauss law gives

$$(4r+26)\big(A_r(h)-B_{r+1}(h)\big)=\Phi(h),$$

and therefore

$$|B_{r+1}(h)-B_r(h)|\le \frac{C}{r}\big(\omega_h(r)+|\Phi(h)|\big). \tag{37}$$

Lemma 5.5 (uniform geometry). *Let Γ be the infinite graph obtained by continuing the stable periodic end. It has bounded degree and is roughly isometric to $\mathbb{Z}^2$. Consequently there are constants $c, C>0$ such that, uniformly in $x\in\Gamma$ and $R\ge 1$,*

$$cR^2\le |B_\Gamma(x,R)|\le CR^2, \tag{38}$$

and, for a fixed dilation factor $\Lambda>1$, the weak graph Poincaré inequality

$$\sum_{v\in B(x,R)}|f(v)-f_{B(x,R)}|^2\le CR^2\sum_{\substack{\{u,v\}\in E(\Gamma)\\ u,v\in B(x,\Lambda R)}}|f(u)-f(v)|^2 \tag{39}$$

holds. Hence there are $\eta>0$ and C_H such that every harmonic function on $B(x,2R)$ satisfies

$$|h(y)-h(z)|\le C_H\left(\frac{d(y,z)}{R}\right)^{\eta}\operatorname{osc}_{B(x,2R)}h,\qquad y,z\in B(x,R). \tag{40}$$

The same hypotheses give the Gaussian heat-kernel estimates used below.

Proof. By Appendix A, outside a uniformly bounded seam strip the graph is exactly two square-lattice staircase sectors. Collapse in each shell the 26 seam states to a bounded cluster and straighten the two staircase coordinates. The resulting map and its coarse inverse distort graph distances by fixed multiplicative and additive constants; hence Γ is roughly isometric to a lattice net in a Euclidean cone of finite positive angle. Such a cone is bi-Lipschitz to the plane after a linear rescaling of its angular coordinate, and any bounded-mesh lattice net in the plane is roughly isometric to $\mathbb{Z}^2$. Thus $\Gamma\simeq_{\mathrm{ri}}\mathbb{Z}^2$. This coarse reparametrization uses shell distance as its radial variable; it is not the natural square-lattice embedding used in the elliptic blow-down below, and therefore does not identify the two scaling problems.

For completeness, the transfer of the Poincaré inequality can be seen directly in this bounded-degree situation. Let $F : \Gamma \to \mathbb{Z}^2$ be a rough isometry and choose a coarse inverse S on the lattice. Fibers of F have uniformly bounded diameter, hence uniformly bounded cardinality. For a function f on a graph ball, put $g(y) = f(Sy)$ on the corresponding lattice ball. If y, y' are neighboring lattice vertices, Sy and Sy' are at uniformly bounded graph distance; joining them by a path of bounded length and using Cauchy–Schwarz gives

$$|g(y) - g(y')|^2 \le C \sum_{e \in \gamma_{y,y'}} |df(e)|^2.$$

Because all paths have bounded length, bounded degree and bounded fibers imply that each graph edge occurs in only $O(1)$ of these comparison paths. The standard $\mathbb{Z}^2$ Poincaré inequality therefore transfers to g, while the difference between $f(v)$ and $g(Fv)$ is controlled in the same way along a uniformly bounded path. Comparing the two means gives (39) for some fixed Λ. The same bounded-fiber comparison of balls gives (38). This is the usual rough-isometry invariance argument; see [5, 4].

Under volume doubling, changing the fixed dilation factor in the weak Poincaré inequality changes only its constant (by the standard finite covering/chaining argument). Delmotte's theorem [6] then gives the parabolic Harnack inequality, Gaussian heat-kernel bounds, and in particular the interior Hölder estimate (40). □

The metric coarse geometry above is plane-like, but the *elliptic scaling limit in the natural square-lattice coordinates* remembers more than that coarse geometry. This is the point at which the similarity factor $\sqrt{5}$ enters.

Let

$$W = \{z = x + iy : x > 0,\ 0 < y < 2x\}, \qquad \theta_0 = \arctan 2, \qquad a = \frac{1}{2}\log 5.$$

At fixed shell parameter x, the two boundary points of one widening wedge are x and $(1+2i)x$. The finite periodic seam and its boundary layer join the four path endpoints at uniformly bounded graph distance, by (A.9a). Thus after rescaling this strip collapses, but the induced boundary identification in the lattice chart is the similarity

$$T(z) = (1 + 2i)z = \sqrt{5}\, e^{i\theta_0} z, \tag{41}$$

not an isometry of the two Euclidean rays.

Definition 5.6 (similarity-welded limit). Let $\mathcal{X}$ be the limiting harmonic problem obtained from two copies W_+, W_- of W by identifying, at each common shell parameter $x > 0$, the four boundary traces carried by the collapsed seam. On each copy the lower to upper boundary identification is (41). Harmonic functions on $\mathcal{X}$ are harmonic in the interiors of $W_\pm$, have the common welded trace, and satisfy the Kirchhoff flux-matching condition across the collapsed seam.

The involution ι interchanging W_+ and W_- preserves this limiting problem. In the symmetric sector, one may keep a single copy of W and identify its boundary rays by T. In the antisymmetric sector the common seam trace is zero, so one obtains the Dirichlet problem on the wedge W.

Lemma 5.7 (compactness and the correct welded limit). *Let $R_j \to \infty$, and let u_j be harmonic on stable graph annuli which, after division of the shell and bulk lattice coordinates by R_j, exhaust compact subsets of $W_+ \sqcup W_-$. Suppose that the normalized u_j are locally uniformly bounded. Then, after passage to a subsequence, their piecewise affine bulk interpolants converge locally uniformly and weakly in H^1_{loc} to a pair $u = (u_+, u_-)$ satisfying*

$$\sum_{\epsilon=\pm} \int_{W_\epsilon} \nabla u_\epsilon \cdot \nabla \varphi_\epsilon \, dA = 0 \tag{42}$$

for every compactly supported test pair $\varphi = (\varphi_+, \varphi_-)$ which is smooth up to the two rays and has the same trace at boundary points identified by the collapsed seam. In particular the two limiting functions are harmonic in the bulk, their four seam traces agree under the similarity welding, and (42) is the Kirchhoff transmission condition. If the discrete fluxes $\Phi(u_j)$ converge to J, the corresponding Kirchhoff flux of u is J.

Proof. We give the compactness and transmission argument because the collapsing seam is the only nonstandard point. On the two bulk paths use the exact lattice coordinates (r, k) from Appendix A, and put $h_j = R_j^{-1}$. Fix compact welded annuli $K \Subset K' \Subset \mathcal{X} \setminus \{0\}$. Choose a graph cutoff η_j which is one over the vertices corresponding to K, vanishes outside K', and satisfies

$$|\eta_j(v) - \eta_j(w)| \leq Ch_j \qquad (v \sim w).$$

Testing the discrete equation $Lu_j = 0$ against $\eta_j^2 u_j$ and using $2ab \leq a^2 + b^2$ gives the standard discrete Caccioppoli inequality

$$\sum_{\{v,w\}\subset K} |u_j(v) - u_j(w)|^2 \leq C \sum_{\{v,w\}\subset K'} \max(|u_j(v)|^2, |u_j(w)|^2)|\eta_j(v) - \eta_j(w)|^2. \quad (43)$$

There are $O(R_j^2)$ bulk edges and only $O(R_j)$ seam/boundary-layer edges in K'. Local boundedness of u_j therefore makes the right hand side of (43) uniformly bounded. Triangulating every square-lattice cell by a fixed diagonal, the affine interpolants on the two bulk wedges consequently have uniformly bounded H^1 norm on K. Together with the graph Hölder estimate (40), this gives, after a diagonal subsequence, weak H^1_{loc} and locally uniform convergence to functions $u_\pm$.

We next identify the traces. Appendix A, (A.9a), gives a constant C_0 such that the four path endpoints associated with one shell parameter are joined in the stable seam strip by graph paths of length at most C_0, with shell index changing by at most C_0. On a macroscopic annulus these paths have rescaled diameter $O(h_j)$. Applying (40) in a graph ball of radius comparable with R_j gives

$$|u_j(e) - u_j(e')| \leq Ch_j^{\eta} \longrightarrow 0$$

for any two such endpoints. Thus the four limiting traces agree. For a single bulk wedge the lower endpoint with shell coordinate x is represented by $z = x$, whereas its upper endpoint is represented by $z = (1 + 2i)x$. Hence the trace identification is exactly $z \sim Tz$ with T from (41).

It remains to prove the transmission law rather than merely trace equality. For a test pair φ as in the statement, define a discrete test function φ_j as follows. On bulk vertices sample $\varphi_\pm$ at the rescaled lattice point. On the seam states in shell r, assign the common welded boundary value at shell parameter r/R_j; the bounded coordinate shifts in the finite boundary layer change this prescription by only $O(h_j)$. Therefore on every edge belonging to the seam or joining the seam to a bulk endpoint,

$$|d\varphi_j| = O(h_j).$$

There are $O(R_j)$ such edges on the support of φ, whence

$$\sum_{e \text{ seam}} |d\varphi_j(e)|^2 = O(R_j h_j^2) = O(R_j^{-1}). \tag{44}$$

The Caccioppoli bound gives $\sum_{e \subset K'} |du_j(e)|^2 = O(1)$, so by Cauchy–Schwarz the contribution of all seam and boundary-layer edges to

$$\mathcal{E}_j(u_j, \varphi_j) := \sum_{\{v,w\} \in E(\Gamma)} (u_j(v) - u_j(w))(\varphi_j(v) - \varphi_j(w))$$

is $O(R_j^{-1/2}) = o(1)$. Since u_j is harmonic and the support of φ_j stays away from the two ends of its annulus, $\mathcal{E}_j(u_j, \varphi_j) = 0$. On the square-lattice bulk the remaining sum is the usual finite-difference Dirichlet form. Weak H^1 convergence and the Riemann-sum identity for the square grid give

$$\lim_{j\to\infty} \mathcal{E}_j(u_j, \varphi_j) = \sum_{\epsilon=\pm} \int_{W_\epsilon} \nabla u_\epsilon \cdot \nabla \varphi_\epsilon \, dA,$$

which proves (42). In particular integration by parts in the two smooth wedge interiors identifies this weak equation with the Kirchhoff sum of normal fluxes along the welded rays.

Finally fix two macroscopic shell sections inside the limiting annulus and choose a welded cutoff χ which is one on the inner section and zero on the outer section. Construct χ_j by the same sampling prescription. Discrete summation by parts, or equivalently telescoping the divergence-free edge current shell by shell, gives exactly

$$\mathcal{E}_j(u_j, \chi_j) = \Phi(u_j)$$

(up to the fixed global sign convention). The seam contribution again tends to zero by (44), while the bulk part converges to the continuum Dirichlet pairing. Therefore the limiting Kirchhoff flux is $\lim_j \Phi(u_j) = J$. $\square$

Lemma 5.8 (spectral gap of the welded limit). *Put*

$$\alpha = \frac{\pi}{\theta_0} = \frac{\pi}{\arctan 2}. \tag{45}$$

Let u be harmonic on $\mathcal{X} \setminus \{0\}$, have zero total flux, and suppose that after addition of a constant

$$|u(z)| \le C\big(\rho^\beta + \rho^{-\beta}\big), \qquad \rho = |z|,$$

for some $0 < \beta < \alpha$. Then u is constant.

Proof. Decompose

$$u = u_{\mathrm{sym}} + u_{\mathrm{anti}}, \qquad u_{\mathrm{sym}} = \tfrac{1}{2}(u + u \circ \iota), \qquad u_{\mathrm{anti}} = \tfrac{1}{2}(u - u \circ \iota).$$

The shell-flux functional is invariant under the wedge-exchange involution, so

$$\Phi(u_{\mathrm{sym}}) = \Phi(u), \qquad \Phi(u_{\mathrm{anti}}) = 0.$$

In particular the symmetric part has zero flux under the hypothesis of the lemma. The antisymmetric part has zero trace on both boundary rays of W. Separation of variables in polar coordinates therefore gives only the Dirichlet wedge modes

$$\rho^{\pm n\pi/\theta_0} \sin \frac{n\pi\vartheta}{\theta_0}, \qquad n \geq 1.$$

The assumed two-sided growth with $\beta < \pi/\theta_0$ forces all of their coefficients to vanish.

For the symmetric part write

$$w = \log z = \xi + i\eta, \qquad c = a + i\theta_0, \qquad a = \frac{1}{2}\log 5.$$

The welding $z \sim Tz$ becomes

$$w \sim w + c.$$

Thus the symmetric sector is the flat cylinder $\mathbb{C}/c\mathbb{Z}$ for the harmonic equation. Introduce orthonormal coordinates parallel and perpendicular to c,

$$s = \frac{a\xi + \theta_0\eta}{|c|}, \qquad t = \frac{\theta_0\xi - a\eta}{|c|}.$$

Then s is periodic modulo $|c|$. The Fourier expansion of a harmonic function on this cylinder consists of the zero mode

$$A_0 + B_0 t$$

and, for $k \geq 1$, modes with exponential factors

$$\exp\left(\pm\frac{2\pi k}{|c|}t\right)$$

multiplied by $\sin(2\pi ks/|c|)$ or $\cos(2\pi ks/|c|)$. Since $0 \le \eta \le \theta_0$ while $\rho = e^{\xi}$, the nonzero k-th Fourier mode has radial power exponent

$$\sigma_k = \frac{2\pi k \theta_0}{a^2 + \theta_0^2}. \tag{46}$$

In particular

$$\sigma_1 = 3.7133569\ldots > \frac{\pi}{\theta_0} = 2.8375525\ldots.$$

(The inequality is equivalent to $\theta_0 > a$.) Hence the growth bound with $\beta < \alpha$ removes every nonzero Fourier mode.

It remains to eliminate the linear zero mode. In the original wedge coordinates

$$t = \frac{\theta_0 \log \rho - a \arg z}{|c|}.$$

Using the longitudinal-flux formula of Section 5.4, a single copy of this function has flux $|c| \neq 0$; the symmetric two-wedge mode has twice that flux. Therefore the zero-total-flux hypothesis forces $B_0 = 0$. Only the constant A_0 remains. □

Lemma 5.9 (zero-flux decay). *Let* h *be harmonic on a stable annulus*

$$R \le r \le N.$$

Let $\Phi(h)$ *be its constant outward flux and put*

$$M = \operatorname{osc}\big(h|_{S_R \cup S_N}\big).$$

For every $0 < \beta < \alpha = \pi/\arctan 2$ *there is* C_β*, independent of* R, N, h*, such that*

$$\omega_h(r) \le C_\beta \left[M \left(\frac{R}{r}\right)^{\beta} + M \left(\frac{r}{N}\right)^{\beta} + |\Phi(h)| \right] \tag{47}$$

for $2R \le r \le N/2$*.*

Proof. Assume the estimate fails for a fixed $\beta < \alpha$. For a counterexample write

$$D(r) = M(R/r)^{\beta} + M(r/N)^{\beta} + |\Phi(h)|$$

and let

$$Q = \max_{2R \le r \le N/2} \frac{\omega_h(r)}{D(r)}.$$

There is then a sequence for which $Q_j \to \infty$; choose a maximizing radius r_j. After subtracting the minimum of the boundary data, the maximum principle puts the whole harmonic function between 0 and M_j, so $\operatorname{osc} h_j \le M_j$. If r_j/R_j stayed bounded, the first term of $D_j(r_j)$ would be a fixed positive multiple of M_j and Q_j would be bounded; similarly $N_j/r_j \to \infty$. Hence

$$\frac{r_j}{R_j} \longrightarrow \infty, \qquad \frac{N_j}{r_j} \longrightarrow \infty. \tag{48}$$

Put $\Omega_j = \omega_{h_j}(r_j)$. Since $\Omega_j = Q_j D_j(r_j)$,

$$\frac{|\Phi(h_j)|}{\Omega_j} \le Q_j^{-1} \longrightarrow 0. \tag{49}$$

Moreover, for every fixed $s > 0$, (48) makes $\lfloor s r_j \rfloor$ admissible for all large j, and maximality gives

$$\frac{\omega_{h_j}(\lfloor s r_j \rfloor)}{\Omega_j} \le \frac{D_j(\lfloor s r_j \rfloor)}{D_j(r_j)} \tag{50}$$

$$\le C \max(s^{\beta}, s^{-\beta}). \tag{51}$$

Normalize

$$\widetilde{h}_j = \frac{h_j - B_{r_j}(h_j)}{\Omega_j}.$$

To obtain an absolute, rather than only oscillation, bound, sum (37). For $s \ge 1$, using (51) and (49),

$$\frac{|B_{\lfloor s r_j \rfloor}(h_j) - B_{r_j}(h_j)|}{\Omega_j} \le C \sum_{t=r_j}^{\lfloor s r_j \rfloor} \frac{(t/r_j)^{\beta} + o(1)}{t} \le C(1 + s^{\beta}),$$

and the same argument inward gives $C(1 + s^{-\beta})$ for $0 < s \le 1$. Since every value on S_t differs from the weighted shell mean by at most $\omega_{h_j}(t)$, the normalized functions are locally uniformly bounded under the rescaling $r \mapsto r/r_j$, with the global two-sided growth bound

$$|\widetilde{h}_j(z)| \le C(\rho^{\beta} + \rho^{-\beta}) \tag{52}$$

on each fixed compact rescaled annulus, after enlarging C once.

Lemma 5.7 therefore gives a subsequential harmonic limit u on $\mathcal{X} \setminus \{0\}$. By (49) its total flux is zero, and (52) passes to the limit. The cross-section corresponding to $r = r_j$ is compact after welding; choosing maximizing and minimizing vertices on that shell and passing to a further subsequence gives

$$\operatorname{osc}_{\{x=1\}} u = 1.$$

Thus u is nonconstant. This contradicts Lemma 5.8, because $\beta < \alpha$. Hence (47) holds. □

Lemma 5.10 (Dirichlet Poincaré on stable annuli). *Let D be a finite stable annulus, including its two boundary shells, and let f vanish on those boundary shells. Extend f by zero to the infinite stable graph Γ. If $d = \max(1, \operatorname{diam} D)$, then*

$$\sum_{v \in D} |f(v)|^2 \leq C d^2 \sum_{\{u,v\} \in E(\Gamma)} |\widetilde{f}(u) - \widetilde{f}(v)|^2. \tag{53}$$

Consequently the first Dirichlet eigenvalue satisfies $\lambda_1(D) \geq c d^{-2}$.

Proof. Fix $x \in D$. By (38), $|D| \leq |B(x, d)| \leq C_0 d^2$. Choose once and for all K so large that $c_0 K^2 \geq 2C_0$, where c_0 is the lower volume-growth constant, and set $B = B(x, Kd)$. Then $|B| \geq 2|D|$, so the zero set $A = B \setminus D$ of $\widetilde{f}$ has $|A| \geq |B|/2$. Let $\bar{f}$ be the mean of $\widetilde{f}$ on B. Since $\widetilde{f} = 0$ on A,

$$|A|\,|\bar{f}|^2 \leq \sum_B |\widetilde{f} - \bar{f}|^2,$$

and therefore

$$\sum_D |f|^2 \leq 2 \sum_B |\widetilde{f} - \bar{f}|^2 + 2|B||\bar{f}|^2 \leq 6 \sum_B |\widetilde{f} - \bar{f}|^2.$$

Apply the global Poincaré inequality (39) to the ball $B(x, Kd)$. Since $\widetilde{f}$ is supported in $D \subset B(x, d)$, every edge on which $d\widetilde{f}$ is nonzero lies in $B(x, d+1) \subset B(x, \Lambda K d)$ (after increasing the fixed K if necessary). Thus the energy on the right is exactly the zero-extension Dirichlet energy, and (53) follows. The Rayleigh quotient gives the eigenvalue bound. Notice that defining the Dirichlet energy by zero extension includes all boundary-crossing edges automatically, so no unproved boundary-density assumption is being used. □

Lemma 5.11 (logarithmic killed Green bound). *Let D be a finite stable annulus of diameter at most Cm, with its two boundary shells grounded. If $G_D = L_D^{-1}$ is the Dirichlet Green kernel, then*

$$\sup_{x,y\in D} |G_D(x,y)| \le C\log(2+m). \tag{54}$$

Proof. We may assume $m \ge 2$. By Lemma 5.5 and Delmotte's Gaussian estimate, the continuous-time heat kernel on the infinite stable graph satisfies

$$H_t(x,x) \le C/t, \qquad t \ge 1.$$

The killed heat kernel is dominated by the unrestricted one, while its ℓ^2 operator norm is at most one. Hence

$$\int_0^1 H_t^D(x,x)\,dt \le 1, \qquad \int_1^{m^2} H_t^D(x,x)\,dt \le C\log m.$$

Lemma 5.10 gives $\lambda_1(D) \ge c/m^2$. For $t \ge m^2$, the semigroup identity and the L^2 operator norm of e^{-sL_D} give

$$\begin{aligned} H_t^D(x,x) &= \left\|H_{t/2}^D(x,\cdot)\right\|_2^2 \\ &\le e^{-\lambda_1(D)(t-m^2)}\left\|H_{m^2/2}^D(x,\cdot)\right\|_2^2 \\ &= e^{-\lambda_1(D)(t-m^2)}H_{m^2}^D(x,x) \\ &\le Cm^{-2}e^{-c(t-m^2)/m^2}. \end{aligned}$$

Its integral over $[m^2,\infty)$ is $O(1)$. Since

$$G_D(x,x) = \int_0^\infty H_t^D(x,x)\,dt,$$

we obtain $G_D(x,x) = O(\log(2+m))$. The positive self-adjoint kernel obeys

$$|G_D(x,y)|^2 \le G_D(x,x)G_D(y,y),$$

which proves (54). □

5.6 A priori oscillation bound on the protected boundary

Put

$$y_m = A_2(m)^{(2)}x_2.$$

In coherent dual coordinates let D_m be the incidence matrix, so that $L_m = D_m^* D_m$ and

$$p_m = L_m^\dagger D_m^* y_m.$$

Lemma 5.12. *There is a constant* C *such that, whenever* $8 \le R \le N \le m/4$,

$$\operatorname{osc}\big(p_m|_{S_R \cup S_N}\big) \le Cm. \tag{55}$$

No information about the terminal cap of $K_3(m)$ *is needed for this estimate.*

Proof. First,

$$D_m p_m = D_m (D_m^* D_m)^\dagger D_m^* y_m$$

is the orthogonal projection of y_m onto $\operatorname{im} D_m$. Therefore

$$\|D_m p_m\|_2 \le \|y_m\|_2. \tag{56}$$

A direct induction through the three stellar moves of one motif gives

$$\#\operatorname{supp} y_m = 6m + 4, \qquad |y_m(\sigma)| = \frac{1}{144} \quad (\sigma \in \operatorname{supp} y_m). \tag{57}$$

For completeness, before the first move of each motif exactly four supported triangles contain the moving edge; the edge subdivision replaces each by two supported triangles. After that move exactly one supported triangle is the center of the triangular subdivision, which replaces it by three supported triangles. The third stellar center meets no supported triangle. Fresh stellar vertices prevent cancellation. Thus every motif increases the support by 6, starting from the four terms in (7). Consequently

$$\|y_m\|_2^2 = \frac{6m+4}{144^2} = O(m). \tag{58}$$

Now let $v, w \in S_R \cup S_N$. By definition of a distance shell, each has a shortest path to τ_* of length at most N. Concatenating the two paths gives a dual path γ from v to w of length at most $2N \le m/2$; it lies entirely on the inner side of the protected outer shell and never uses the terminal cap. Hence Cauchy–Schwarz and (56)–(58) give

$$|p_m(v) - p_m(w)| \le |\gamma|^{1/2} \|D_m p_m\|_2 = O(\sqrt{m})O(\sqrt{m}) = O(m).$$

Taking the supremum over $v, w \in S_R \cup S_N$ proves (55). $\square$

5.7 Protected middle annuli

Proposition 5.13. *Let σ_r be a fixed seam state transported by the canonical shift. For even m and uniformly for*

$$m^{2/5} \leq r \leq \frac{1}{2}m^{3/5}, \tag{59}$$

one has

$$p_m(\sigma_{2r}) - p_m(\sigma_r) = \lambda \log 2 + o(1). \tag{60}$$

Consequently there are two tetrahedra τ_m^-, τ_m^+ in the stable end such that

$$|p_m(\tau_m^+) - p_m(\tau_m^-)| \geq \frac{\lambda}{5}\log m - O(1). \tag{61}$$

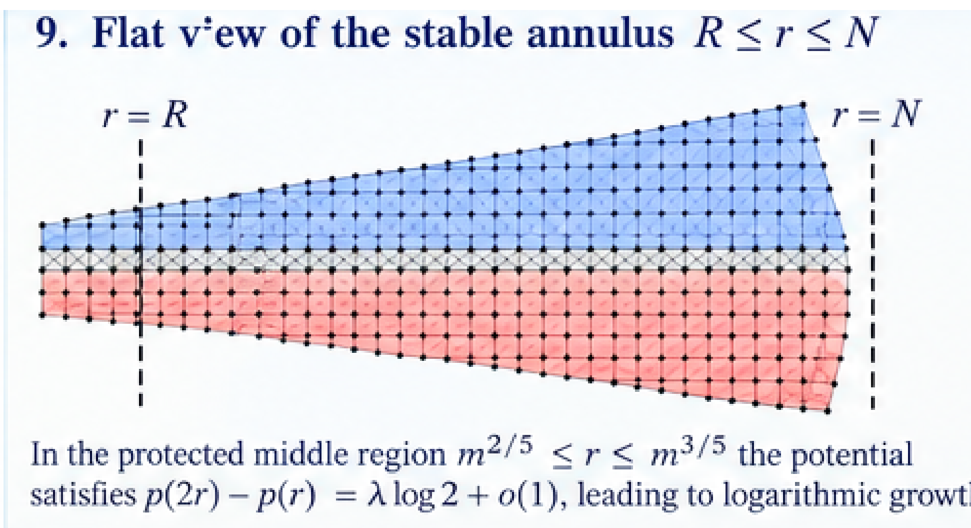

Figure 9: Flattened protected annulus. The proof uses only radii $m^{2/5} \leq r \leq m^{3/5}$, where the influence of both the fixed inner core and the finite outer cap tends to zero. On every dyadic subannulus the increment is $\lambda \log 2 + o(1)$.

Proof. Set

$$R_0 = m^{1/100}, \qquad N_0 = \lfloor m/4 \rfloor,$$

and restrict the parametrix P of Lemma 5.4 to the stable annulus $R_0 \leq r \leq N_0$. Put

$$e = LP - q.$$

By (33),

$$\|e\|_1 \leq C \sum_{r \geq R_0} r^{-2} = O(R_0^{-1}). \tag{62}$$

Let w solve

$$Lw = e$$

on this finite annulus with zero boundary values. Lemma 5.11 gives

$$\sup_{x,y} G_{R_0,N_0}(x,y) \leq C \log m.$$

Hence by (62)

$$\|w\|_\infty \leq C \frac{\log m}{R_0} = o(1). \tag{63}$$

Now define

$$h_m = p_m - P + w.$$

Then $Lh_m = 0$ on the annulus. Lemma 5.12, the logarithmic growth of P, and (63) imply that the oscillation of its boundary data is $O(m)$. Moreover (13) and (34) leave a flux discrepancy $O(R_0^{-1})$. The boundary flux of w is also $O(\|e\|_1)$: if ψ is the harmonic measure which is 1 on the inner boundary and 0 on the outer boundary, discrete Green's identity gives

$$\Phi_{\mathrm{in}}(w) = \sum_v e(v)\psi(v), \qquad 0 \leq \psi \leq 1.$$

Thus (62) gives

$$|\Phi(h_m)| = O(R_0^{-1}). \tag{64}$$

Choose

$$\beta = \frac{13}{5}.$$

Since

$$\tan \frac{3\pi}{8} = 1 + \sqrt{2} > 2,$$

we have $\arctan 2 < 3\pi/8$, and therefore

$$\alpha = \frac{\pi}{\arctan 2} > \frac{8}{3} > \frac{13}{5} = \beta.$$

Lemma 5.9, with boundary amplitude $M = O(m)$, gives for $m^{2/5} \le r \le m^{3/5}$

$$\begin{aligned}\omega_{h_m}(r) &\le C\left[m\left(\frac{m^{1/100}}{r}\right)^{13/5} + m\left(\frac{r}{m}\right)^{13/5} + m^{-1/100}\right]\\ &= o(1),\end{aligned}$$

uniformly in that range. Indeed at the two extremal powers the first two terms are respectively $O(m^{-7/500})$ and $O(m^{-1/25})$.

Equation (37), together with (64), now gives uniformly on a dyadic subannulus in (59)

$$B_{2r}(h_m) - B_r(h_m) = o(1).$$

Since the angular oscillation is also $o(1)$,

$$h_m(\sigma_{2r}) - h_m(\sigma_r) = o(1). \tag{65}$$

By (63) and (35), this proves (60).

Finally choose dyadic radii r_- and r_+ with

$$r_- = m^{2/5+o(1)}, \qquad r_+ = m^{3/5+o(1)}.$$

There are

$$\frac{1}{5}\log_2 m + O(1)$$

dyadic steps between them. The preceding estimates are quantitative: the error in each step is $O(m^{-7/500} + m^{-1/100}\log m)$, hence their sum over $O(\log m)$ steps is $o(1)$. Telescoping (60) gives

$$p_m(\sigma_{r_+}) - p_m(\sigma_{r_-}) = \lambda\log(r_+/r_-) + O(1) = \frac{\lambda}{5}\log m + O(1).$$

Taking $\tau_m^- = \sigma_{r_-}$ and $\tau_m^+ = \sigma_{r_+}$ proves (61). □

5.8 The Euler cocycle

Theorem 5.14 (explicit logarithmic unboundedness). *For all sufficiently large even* m *there is a tetrahedron* $\tau_m \subset K_3(m)$ *such that, after performing*

$$N_m = F_m$$

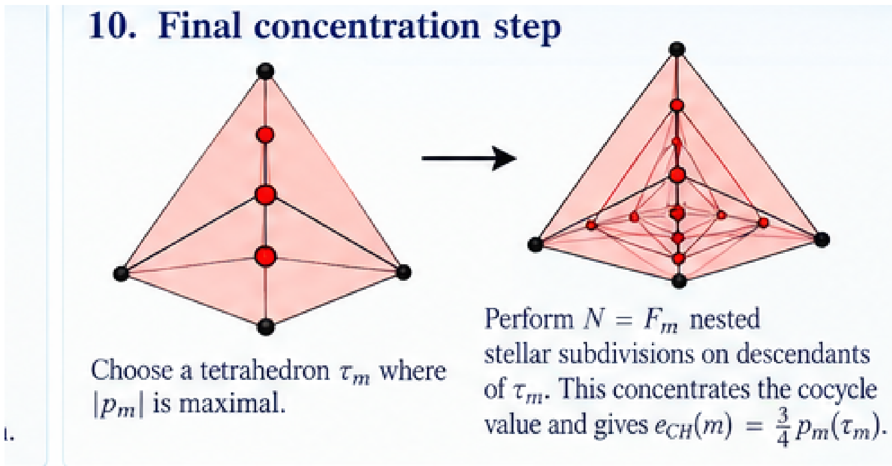

Figure 10: Final concentration step. Choose a tetrahedron τ_m at which $|p_m|$ is maximal, then perform $N = F_m$ nested stellar subdivisions on its descendants. The final averaging gives exactly $e_{CH}(m) = \frac{3}{4}p_m(\tau_m)$.

nested stellar subdivisions of descendants of τ_m*, the resulting fourth subdivision arrow*

$$A_3(m) : K_3(m) \longrightarrow K_4(m)$$

satisfies

$$|e_{CH}(m)| \geq \frac{3\lambda}{40} \log m - O(1), \tag{66}$$

where λ *is given by* (21)*. In particular*

$$\sup |e_{CH}| = \infty \tag{67}$$

on chains consisting entirely of iterated stellar subdivisions (equivalently, of stellar aggregation arrows in the opposite refinement direction).

Moreover

$$f_3(K_4(m)) = 4F_m = 2m^2 + 42m + 48,$$

and hence

$$|e_{CH}(m)| \geq \frac{3\lambda}{80} \log f_3(K_4(m)) - O(1). \tag{68}$$

Proof. By Proposition 5.13, two tetrahedra τ_m^-, τ_m^+ satisfy

$$|p_m(\tau_m^+) - p_m(\tau_m^-)| \geq \frac{\lambda}{5} \log m - O(1).$$

Therefore at least one of them, call it τ_m, satisfies

$$|p_m(\tau_m)| \geq \frac{\lambda}{10} \log m - O(1). \tag{69}$$

A stellar subdivision of a tetrahedron replaces one descendant by four descendants, all carrying the same coherently oriented coefficient. After N nested tetrahedral subdivisions of τ_m, its multiplicity in the final top-cell average is $1 + 3N$, while every other old tetrahedron retains multiplicity 1. Since

$$\sum_{\tau} p_m(\tau) = 0,$$

the final normalized projection is exactly

$$e_{CH} = \frac{3N}{F_m + 3N} p_m(\tau_m). \tag{70}$$

For $N = F_m$ this gives

$$e_{CH}(m) = \frac{3}{4} p_m(\tau_m).$$

Together with (69) this proves (66) and hence (67).

Finally each tetrahedral stellar subdivision adds three tetrahedra, so

$$f_3(K_4(m)) = F_m + 3F_m = 4F_m = 2m^2 + 42m + 48.$$

Thus

$$\log m = \frac{1}{2} \log f_3(K_4(m)) + O(1),$$

and (68) follows. □

The explicit lower-bound constants are

$$\frac{3\lambda}{40} = 0.000894919281663899\ldots, \qquad \frac{3\lambda}{80} = 0.000447459640831949\ldots.$$

Status of the proof. The argument above reduces Theorem 5.14 to explicit finite incidence identities and the stated graph elliptic lemmas. In particular, the similarity-welded compactness lemma is proved through the discrete Dirichlet form, including the vanishing seam-energy estimate, and the Dirichlet spectral gap used for the killed Green kernel is derived explicitly from the global Poincaré inequality by zero extension. The 26–state and 32–state identities are exact integer/rational calculations; their complete finite certificates are collected in Appendices B and C. The compatibility condition (31) and connectedness of the enlarged first-order cell are the only algebraic facts needed for the parametrix; the cofactor (29) is an independent integer certificate. Lemmas 5.5–5.11 are standard consequences of volume doubling and Poincaré inequality on the stable graph, while Lemma 5.7 identifies the correct similarity welding left by the collapsed seam. No numerical asymptotic estimate is used in Theorem 5.14.

Analytic references. The graph Harnack and Gaussian heat-kernel estimates used above are standard consequences of volume doubling and the scale-invariant Poincaré inequality; we use Delmotte [6]. For square/orthogonal lattice scaling limits one may compare Courant–Friedrichs–Lewy [3] and Skopenkov [14]. No numerical asymptotic estimate is used in Theorem 5.14.

6 Bounded cohomology, ℓ^1–homology, and Ivanov's obstruction

This section is logically independent of the explicit periodic construction. It explains a conceptual reason why one should expect the universal Euler class to require unbounded representatives. It also explains exactly why this observation alone is not a proof about a cocycle defined on an arbitrary category nerve.

6.1 Bounded singular cochains and the comparison map

Let X be a topological space. Write $S_k(X)$ for the set of singular k–simplices and

$$C_k(X;\mathbb{R}) = \left\{ \sum_j a_j \sigma_j : \text{finite sums} \right\}.$$

The ℓ^1–norm of a singular chain is

$$\left\| \sum_j a_j \sigma_j \right\|_1 = \sum_j |a_j|.$$

For a homology class $\alpha \in H_k(X;\mathbb{R})$ its ℓ^1–seminorm is

$$\|\alpha\|_1 = \inf\{\|z\|_1 : z \text{ is a cycle representing } \alpha\}. \tag{71}$$

A singular cochain $c \in C^k(X;\mathbb{R})$ is *bounded* if

$$\|c\|_\infty = \sup_{\sigma \in S_k(X)} |c(\sigma)| < \infty.$$

Bounded cochains form a subcomplex $C_b^*(X;\mathbb{R})$, and its cohomology is the bounded cohomology $H_b^*(X;\mathbb{R})$. Inclusion of complexes gives the comparison map

$$\mathrm{comp} : H_b^k(X;\mathbb{R}) \longrightarrow H^k(X;\mathbb{R}). \tag{72}$$

For any bounded cochain and finite chain,

$$|\langle c, z\rangle| \leq \|c\|_\infty \, \|z\|_1. \tag{73}$$

This elementary inequality is the analytic content behind the duality between bounded cohomology and the ℓ^1–seminorm; see Gromov [8] and modern treatments such as [7].

6.2 Ivanov's vanishing theorem

The following is one of the basic theorems of bounded cohomology.

Theorem 6.1 (Gromov–Ivanov mapping/vanishing theorem). *Let X be a path-connected countable CW complex. Bounded cohomology with trivial real coefficients depends only on $\pi_1(X)$: the canonical map to a classifying space of the fundamental group induces an isometric isomorphism. In particular, if $\pi_1(X)$ is amenable, then*

$$H_b^k(X;\mathbb{R}) = 0 \qquad (k \geq 1).$$

In particular this holds for every simply connected X.

Gromov introduced the general framework in [8]. Ivanov gave a homological-algebra proof, including the vanishing theorem for simply connected spaces, in [10, 11]. A complete modern multicomplex treatment, including the isometric comparison between singular and simplicial bounded cohomology for complete multicomplexes, is given in [7].

6.3 The elementary bounded-homology argument on S^4

For the Euler class one can see the obstruction without using the full mapping theorem.

Lemma 6.2. *For* $n \geq 1$*,*

$$\|[S^n]\|_1 = 0.$$

Proof. For every integer $d > 1$ there is a self-map $f_d : S^n \to S^n$ of degree d. Functoriality of the ℓ^1–seminorm and homogeneity give

$$d\|[S^n]\|_1 = \|d[S^n]\|_1 = \|(f_d)_*[S^n]\|_1 \leq \|[S^n]\|_1.$$

Hence $\|[S^n]\|_1 = 0$. □

Theorem 6.3 (Ivanov–Gromov bounded-homology obstruction for the Euler class). *Let* $\mathscr{B}^+_{S^3}$ *be a classifying space for oriented PL* S^3*–bundles, and let* $e_{PL} \in H^4(\mathscr{B}^+_{S^3}; \mathbb{R})$ *be the universal Euler class. No bounded singular cocycle represents* e_{PL}*.*

Proof. An oriented real 4–plane bundle has an oriented unit 3–sphere bundle, so there is a natural classifying map

$$j : BSO(4) \longrightarrow \mathscr{B}^+_{S^3}.$$

By naturality of the Euler class,

$$j^* e_{PL} = e \in H^4(BSO(4); \mathbb{R}),$$

the ordinary universal Euler class of oriented 4–plane bundles. This class is nonzero. For example, there is a map

$$f : S^4 \longrightarrow BSO(4)$$

classifying the quaternionic Hopf line bundle (viewed as an oriented real 4–plane bundle) for which, after choosing orientations,

$$\langle f^*e, [S^4]\rangle = 1.$$

Suppose c were a bounded singular cocycle on $\mathscr{B}^+_{S^3}$ representing e_{PL}. Then $(j \circ f)^*c$ is bounded and represents f^*e. By (73) and Lemma 6.2,

$$1 = |\langle (j \circ f)^*c, [S^4]\rangle| \leq \|c\|_\infty \, \|[S^4]\|_1 = 0,$$

a contradiction. □

Remark 6.4 (Ivanov's theorem gives the same contradiction). Since $BSO(4)$ is simply connected, Theorem 6.1 gives

$$H^4_b(BSO(4); \mathbb{R}) = 0.$$

If e_{PL} were in the image of the comparison map on $\mathscr{B}^+_{S^3}$, its pullback e would lie in the image of the comparison map on $BSO(4)$, which is impossible. This is the bounded-cohomology form of the same argument.

6.4 Application to the aggregation classifying space

Mnëv's 2007 theorem identifies the classifying space of the category of combinatorial manifolds of a fixed PL type and aggregation morphisms with the classifying space of the corresponding simplicial PL homeomorphism group [12]. In the oriented spherical setting, the universal Euler class is represented by the aggregation local cocycle of [13]. Thus, at the level of *ordinary* cohomology, the category nerve carries exactly the class to which Theorem 6.3 applies.

There is nevertheless a bounded-cohomology subtlety.

Remark 6.5 (Why a bounded nerve cocycle is not automatically a bounded singular cocycle). Let K be an arbitrary simplicial set or category nerve. A bounded simplicial cochain on K is a bounded function on the simplices of K. The geometric realization map identifies ordinary simplicial cohomology with ordinary singular cohomology, but the usual proof uses subdivision and simplicial approximation and is not automatically bounded in the ℓ^1/ℓ^∞

norms. Therefore

$$\text{“c bounded on simplices of K”}$$

$$\not\Rightarrow$$

$$\text{“the corresponding singular class has a bounded representative.”}$$

without an additional norm-controlled comparison theorem.

For large complete multicomplexes such a theorem *is* available: Gromov's Isometry Lemma identifies simplicial bounded cohomology with singular bounded cohomology isometrically; see [8, 7]. An arbitrary category nerve is not automatically such a complete multicomplex.

This yields the following useful conditional statement.

Theorem 6.6 (Conditional Ivanov theorem for an aggregation nerve). *Let $\mathcal{C}$ be an oriented aggregation category whose classifying space carries the universal oriented PL S^3 Euler class, and suppose there is a norm-controlled comparison from bounded simplicial cochains of $N\mathcal{C}$ to bounded singular cochains of $|N\mathcal{C}|$ which:*

- *(i) induces the usual simplicial–singular identification in ordinary cohomology;*
- *(ii) sends a simplicial cocycle of finite ℓ^∞ norm to a singular bounded cocycle (with norm bounded by a constant multiple of the simplicial norm).*

Then no simplicial cocycle on $N\mathcal{C}$ representing the universal Euler class can be uniformly bounded. In particular, under this comparison hypothesis, e_{CH} is unbounded.

Proof. A bounded simplicial representative would be sent to a bounded singular representative of the same universal Euler class. This contradicts Theorem 6.3. □

The explicit Theorem 5.14 proved in the preceding section is stronger for the particular cocycle e_{CH}: it establishes unboundedness directly, without any bounded-comparison hypothesis on the category nerve.

6.5 What a hypothetical uniform local bound would imply for triangulated bundles

Let an oriented PL S^3–bundle over an ordered triangulated closed oriented 4–manifold B be encoded by a local system of spherical aggregations. On each oriented 4–simplex σ of B, restriction to the ordered flag of vertices produces a chain of four aggregation arrows, denoted $\mathcal{S}_\sigma$. The local formula satisfies

$$\langle e(E), [B] \rangle = \sum_{\sigma \in B(4)} \varepsilon(\sigma)\, e_{CH}(\mathcal{S}_\sigma), \qquad \varepsilon(\sigma) = \pm 1. \tag{74}$$

This is precisely the meaning of e_{CH} being a local cocycle representing the Euler class; see [13].

If there were a global bound

$$|e_{CH}(\mathcal{S})| \leq M$$

for all four-arrow chains, then (74) would give

$$|\langle e(E), [B] \rangle| \leq M f_4(B). \tag{75}$$

For a bundle over S^4 with Euler number E, this would force

$$f_4(B) \geq |E|/M.$$

The explicit unboundedness theorem shows that no such finite universal M exists for the Hodge cocycle e_{CH}. This does *not* rule out other complexity estimates for triangulated sphere bundles, nor does it rule out a different local representative with useful bounds on a restricted class of chains. It says specifically that the global sup-norm strategy cannot use this Hodge representative with a finite universal constant.

7 Conclusions and questions

The constructive and bounded-cohomological viewpoints now fit together as follows.

1. The universal Euler class is intrinsically outside the image of singular bounded cohomology; this is already visible on the linear subfamily $BSO(4)$ by Ivanov–Gromov theory.

2. The aggregation Hodge cocycle e_{CH} is not merely abstractly forced to be complicated: the explicit periodic stellar family exhibits logarithmic growth and identifies the geometric mechanism responsible for it.

3. The growth comes from a marginal logarithmic mode of a two-dimensional periodic electrical end. The exact seam cell fixes a nonzero coefficient, while the first nonconstant zero-flux exponent of the similarity-welded limit $\pi/\arctan 2 > 2$ protects the middle scales from arbitrary finite boundary conditions.

4. A separate categorical problem is to understand which subcategories of aggregations (for example, those generated by stellar aggregations) retain the full universal classifying-space homotopy type. That question is not used in the proof above.

A All-radius stable periodic combinatorics

This appendix supplies the all-radius combinatorial statement used in Section 5.2. It separates the genuinely finite part of the verification from the induction in the shell radius.

A.1. Stellar labels

Number the three new vertices in the j-th motif, $j = 0, 1, 2, \ldots$, by

$$u_j = 3j + 7, \qquad v_j = 3j + 8, \qquad w_j = 3j + 9.$$

For $j \geq 2$ the moving tetrahedron before motif j is

$$T_j = (3j + 1, 3j + 4, 3j + 5, 3j + 6),$$

and the three stellar centers are

$$(3j + 1, 3j + 4), \qquad (3j + 4, 3j + 5, 3j + 7), \qquad (3j + 6, 3j + 8).$$

The elementary replacement rule is the following: if a tetrahedron τ contains a stellar center F and the new vertex is v, then τ is replaced by

$$\left\{ (\tau \setminus \{a\}) \cup \{v\} : a \in F \right\}. \tag{A.1}$$

Thus all assertions below can be checked using only equality of vertex labels and the rule that two tetrahedra are dual-adjacent exactly when they have three vertices in common.

Moving-edge fan lemma. For every $j \geq 2$, immediately before motif j the moving edge is

$$E_j = (3j + 1, 3j + 4)$$

and its simplicial link is the cycle

$$0,\ 2,\ 1,\ 3j + 5,\ 3j + 6,\ 3j + 3,\ 3j, \ldots,\ 12,\ 9,\ 0. \tag{A.1a}$$

In particular the degree of E_j is $j + 4$.

Indeed, for $j = 2$ the link is $0, 2, 1, 11, 12, 9, 0$, which follows directly from the first two motifs. Assume (A.1a) for j and write $(a, b, c, d) = (3j+1, 3j+4, 3j+5, 3j+6)$. After the first move, with new vertex $u = 3j + 7$, the next moving edge (b, u) initially has the same link cycle: every tetrahedron (a, b, x, y) is replaced by a child (b, u, x, y). The second move is the stellar subdivision of (b, c, u) with new vertex $v = 3j + 8$; in the link of (b, u) it replaces the subpath $1 - c - d$ by $1 - v - d$. The third move subdivides (d, v) with new vertex $w = 3j+9$; in the same link it replaces the edge $v - d$ by $v - w - d$. Hence the link of the next moving edge is

$$0, 2, 1, v, w, d, 3j + 3, 3j, \ldots, 12, 9, 0,$$

which is exactly (A.1a) with j replaced by $j + 1$. This proves the lemma by induction. It also gives directly the edge-degree formula used in (8).

A.2. Explicit bulk paths

For $r \geq 8$ set

$$A_r = 6r - 23, \qquad B_r = 6r - 17, \qquad C_r = 6r - 14, \qquad D_r = 6r - 8.$$

The positive bulk path is

$$P_r^+ = \{\pi_{r,k}^+ : 0 \leq k \leq 2r - 10\},$$

where

$$\begin{aligned} \pi_{r,k}^+ &= (9 + 3k, 12 + 3k, A_r, B_r), & 0 \leq k \leq 2r - 12, \\ \pi_{r,2r-11}^+ &= (A_r - 1, A_r, A_r + 2, B_r), \\ \pi_{r,2r-10}^+ &= (A_r, A_r + 2, A_r + 5, B_r). \end{aligned}$$

Hence $|P_r^+| = 2r - 9$.

It is convenient to orient the negative bulk path from its fixed-label end toward the moving end. Put

$$P_r^- = \{\pi_{r,k}^- : 0 \leq k \leq 2r - 11\},$$

where

$$\begin{aligned} \pi_{r,k}^- &= (24 + 3k, 27 + 3k, C_r, D_r), & 0 \leq k \leq 2r - 14, \\ \pi_{r,2r-13}^- &= (C_r - 1, C_r, C_r + 2, D_r), \\ \pi_{r,2r-12}^- &= (C_r, C_r + 2, C_r + 5, D_r), \end{aligned}$$

$$\pi^-_{r,2r-11} = (C_r, C_r+1, C_r+2, C_r+5).$$

Thus $|P^-_r| = 2r-10$.

The occurrence of these bulk tetrahedra in the stellar complex follows from the moving-edge fan lemma. For P^+_r use the first move in block $j = 2r-8$: here $a_j = A_r$ and $u_j = B_r$, and the long link arc

$$9, 12, 15, \dots, 6r-24, 6r-21, 6r-18$$

in (A.1a) produces precisely the children (a_j, u_j, x, y) listed as P^+_r. For P^-_r use the first move in block $j = 2r-5$: then $a_j = C_r$, $u_j = D_r$, and the corresponding link arc beginning at 24 produces all states of P^-_r except its last boundary state. That last state

$$(C_r, C_r+1, C_r+2, C_r+5)$$

is produced by the third move of block $j = 2r-6$. Substitution in the later stellar centers shows that none of these displayed bulk states is subsequently subdivided. Thus the formulas describe actual tetrahedra of $K_3(m)$ whenever the indicated blocks have occurred.

Consecutive tetrahedra in either displayed list share a triangle and there are no other same-shell adjacencies among bulk tetrahedra. The generic radial adjacencies are

$$\pi^+_{r,k} \sim \pi^+_{r+1,k}, \qquad 0 \le k \le 2r-10, \tag{A.2}$$
$$\pi^-_{r,k} \sim \pi^-_{r+1,k}, \qquad 0 \le k \le 2r-12. \tag{A.3}$$

The remaining radial adjacency at the moving end of P^-_r is

$$\pi^-_{r,2r-11} \sim \sigma_4(r+1). \tag{A.4}$$

These formulas display directly the two square-lattice staircases: P^+ gains two states at its moving end from r to $r+1$, while on P^- all but the last state continue radially and the finite moving-end boundary layer is renewed.

A.3. Explicit 26-state seam

Write $\sigma_i(r)$ for the seam state with index i. The complete list is as follows; the last column is $144q(\sigma_i(r))$.

i	$\sigma_i(r)$	$144q$
0	$(0, 2, 6r-29, 6r-23)$	0
1	$(0, 9, 6r-23, 6r-17)$	-1
2	$(1, 2, 6r-23, 6r-17)$	0
3	$(6r-23, 6r-19, 6r-18, 6r-17)$	1
4	$(6r-19, 6r-18, 6r-17, 6r-15)$	0
5	$(6r-19, 6r-17, 6r-16, 6r-15)$	1
6	$(6r-17, 6r-16, 6r-15, 6r-12)$	0
7	$(6r-17, 6r-16, 6r-13, 6r-12)$	1
8	$(1, 6r-17, 6r-13, 6r-11)$	0
9	$(1, 6r-13, 6r-11, 6r-10)$	-1
10	$(6r-14, 6r-13, 6r-10, 6r-9)$	1
11	$(21, 24, 6r-14, 6r-8)$	0
12	$(1, 6r-11, 6r-10, 6r-7)$	-1
13	$(6r-10, 6r-9, 6r-8, 6r-6)$	0
14	$(6r-10, 6r-8, 6r-7, 6r-6)$	1
15	$(1, 6r-8, 6r-7, 6r-4)$	-1
16	$(18, 21, 6r-8, 6r-2)$	0
17	$(6r-8, 6r-4, 6r-3, 6r-2)$	1
18	$(1, 6r-4, 6r-2, 6r-1)$	-1
19	$(1, 6r-2, 6r+2, 6r+4)$	0
20	$(15, 18, 6r-2, 6r+4)$	0
21	$(1, 2, 6r+4, 6r+10)$	0
22	$(12, 15, 6r+4, 6r+10)$	0
23	$(0, 2, 6r+10, 6r+16)$	0
24	$(9, 12, 6r+10, 6r+16)$	0
25	$(0, 9, 6r+16, 6r+22)$	-1

In particular $|\Sigma_r| = 26$, all stable source terms are in the seam, and

$$\sum_{i=0}^{25} q(\sigma_i(r)) = 0. \tag{A.5}$$

For completeness, the following birth table makes occurrence of the seam states under the stellar motif explicit. Here M_1, M_2, M_3 mean respectively the first edge, middle triangle, and last edge move of a motif. In row i, put $j = 2r + (j - 2r)$ as indicated. Immediately before the listed move the displayed parent tetrahedron is present; it contains the stellar center of that move, and replacing the displayed omitted vertex by the new stellar vertex gives exactly $\sigma_i(r)$. Every displayed parent is either a tetrahedron in the moving-edge fan (A.1a) or is produced by an earlier move among the finitely many neighboring blocks. Direct substitution also shows that no later stellar center is contained in $\sigma_i(r)$. Hence the table is a symbolic finite verification valid for every r, not a numerical check at one radius.

i	$j-2r$	move	parent tetrahedron	omitted vertex
0	-10	M_1	$(0,2,6r-29,6r-26)$	$6r-26$
1	-8	M_1	$(0,9,6r-23,6r-20)$	$6r-20$
2	-8	M_1	$(1,2,6r-23,6r-20)$	$6r-20$
3	-8	M_1	$(6r-23,6r-20,6r-19,6r-18)$	$6r-20$
4	-8	M_3	$(6r-19,6r-18,6r-17,6r-16)$	$6r-16$
5	-8	M_3	$(6r-19,6r-18,6r-17,6r-16)$	$6r-18$
6	-7	M_3	$(6r-17,6r-16,6r-15,6r-13)$	$6r-13$
7	-7	M_3	$(6r-17,6r-16,6r-15,6r-13)$	$6r-15$
8	-6	M_1	$(1,6r-17,6r-14,6r-13)$	$6r-14$
9	-6	M_2	$(1,6r-14,6r-13,6r-11)$	$6r-14$
10	-6	M_3	$(6r-14,6r-13,6r-12,6r-10)$	$6r-12$
11	-5	M_1	$(21,24,6r-14,6r-11)$	$6r-11$
12	-5	M_2	$(1,6r-11,6r-10,6r-8)$	$6r-8$
13	-5	M_3	$(6r-10,6r-9,6r-8,6r-7)$	$6r-7$
14	-5	M_3	$(6r-10,6r-9,6r-8,6r-7)$	$6r-9$
15	-4	M_2	$(1,6r-8,6r-7,6r-5)$	$6r-5$
16	-3	M_1	$(18,21,6r-8,6r-5)$	$6r-5$
17	-3	M_1	$(6r-8,6r-5,6r-4,6r-3)$	$6r-5$
18	-3	M_2	$(1,6r-5,6r-4,6r-2)$	$6r-5$
19	-1	M_1	$(1,6r-2,6r+1,6r+2)$	$6r+1$
20	-1	M_1	$(15,18,6r-2,6r+1)$	$6r+1$
21	$+1$	M_1	$(1,2,6r+4,6r+7)$	$6r+7$
22	$+1$	M_1	$(12,15,6r+4,6r+7)$	$6r+7$
23	$+3$	M_1	$(0,2,6r+10,6r+13)$	$6r+13$
24	$+3$	M_1	$(9,12,6r+10,6r+13)$	$6r+13$
25	$+5$	M_1	$(0,9,6r+16,6r+19)$	$6r+19$

The same-shell seam edges are

$$34, 45, 56, 67, 89, 9\,12, 13\,14, \tag{A.6}$$

where, for example, 34 denotes the edge $\sigma_3(r)\sigma_4(r)$. The four same-shell bulk attachments are

$$\sigma_1(r) \sim \pi^+_{r,0}, \quad \sigma_3(r) \sim \pi^+_{r,2r-10}, \quad \sigma_{11}(r) \sim \pi^-_{r,0}, \quad \sigma_{10}(r) \sim \pi^-_{r,2r-11}. \tag{A.7}$$

The seam-to-seam incoming and outgoing state numbers are exactly the "in-states" and "out-states" columns of Appendix B; those columns are independent of r. The radial seam-to-bulk exceptions are

$$\sigma_4(r) \sim \pi^+_{r+1,2r-9}, \qquad \sigma_6(r) \sim \pi^+_{r+1,2r-8}, \tag{A.8}$$

$$\sigma_{13}(r) \sim \pi^-_{r+1,2r-11}, \qquad \sigma_{17}(r) \sim \pi^-_{r+1,2r-10}, \qquad \sigma_{14}(r) \sim \pi^-_{r+1,2r-9}. \tag{A.9}$$

Equations (A.2)–(A.9), together with the seam in/out columns in Appendix B, account for all four triangular faces of every state in the stable shell. In particular no unlisted dual edge leaves a stable shell by more than one radial level.

We also record a finite transverse-diameter consequence used below. If e_1, e_2 are the two endpoints of P^+_r and e_3, e_4 those of P^-_r, the displayed adjacency formulas give paths in the stable strip satisfying

$$d(e_i, e_j) \le 17 \qquad (1 \le i, j \le 4). \tag{A.9a}$$

The paths leave the shell index r by at most seven levels. This is a finite check in the periodic seam/boundary-layer incidence table, and after the affine label shift the same finite paths work for every stable r. Only uniform boundedness, not the number 17, is used in the scaling argument.

A.4. The induction

We now justify that these lists are the graph-distance shells, rather than merely a collection of tetrahedra with the desired local incidence.

The shell S_8 is a finite base case. Substitution of $r = 8$ in the formulas above gives $7 + 6 + 26 = 39$ tetrahedra. Direct face comparison in the finite stellar complex gives exactly the distance-8 shell from $\tau_* = (0, 9, 16, 22)$ and gives cumulative source $-8/144 = -1/18$ through that shell. No asymptotic or numerical linear algebra enters this base check.

Assume the formulas describe the distance-r shell. The generic bulk relations (A.2)–(A.4), the finite seam in/out table, and the five exceptional relations (A.8)–(A.9) list every neighbor of S_r not already in $S_{r-1} \cup S_r$. Those unvisited neighbors are exactly the tetrahedra listed above for P^+_{r+1}, P^-_{r+1}, and Σ_{r+1}. Conversely, every tetrahedron in those three lists has at least one listed inward neighbor. Because the neighbor list accounts for all four faces of every tetrahedron, there is no additional unvisited neighbor and no shortcut from a later layer. Hence their graph distance from τ_* is exactly $r+1$. This proves

$$S_r = P^+_r \sqcup P^-_r \sqcup \Sigma_r \qquad (r \geq 8) \tag{A.10}$$

for every shell for which the required stellar labels have been created.

For completeness, the occurrence of the tetrahedra themselves in the stellar complex follows by the same finite recurrence. Advancing r by one advances all moving labels by 6, i.e. by two motif blocks. Substitute the three centers displayed in A.1 for motif indices j and $j+1$ into the stellar replacement rule (A.1). Away from the five boundary states in (A.4),(A.8),(A.9), the listed tetrahedra persist and the two new staircase states are created at the moving end. At the boundary, the replacement rule is exactly (A.4),(A.8),(A.9) and the seam-to-seam in/out table. Thus the finite incidence pattern reproduces itself after two motif blocks.

The largest stellar label appearing in the shell formulas is $6r+22$. After m motifs the largest created vertex is $3m+6$. Thus for even m the entire displayed shell has been created whenever

$$6r + 22 \leq 3m + 6,$$

which is exactly $r \leq m/2 - 3$. The two-block recurrence also shows that no later stellar center is contained in one of the displayed stable tetrahedra, so these tetrahedra persist in $K_3(m)$.

It follows at once from (A.10) that

$$|S_r| = (2r-9) + (2r-10) + 26 = 4r + 7. \tag{A.11}$$

Every bulk state has one outgoing radial edge, so the two bulk paths contribute $4r-19$ edges to the cut. The seam table has total outgoing radial degree 45 (including the five seam-to-bulk edges (A.8)–(A.9)). Hence

$$|C_r| = 4r - 19 + 45 = 4r + 26. \tag{A.12}$$

Finally (A.5), together with the finite base value at $r = 8$, gives

$$\sum_{\tau \in S_r} q(\tau) = 0, \qquad \sum_{d(\tau_*,\tau) \leq r} q(\tau) = -\frac{1}{18} \tag{A.13}$$

for every stable r.

B Exact 26–state seam certificate

This appendix records the complete finite data used in the periodic seam calculation of Section 5.2. The displayed tetrahedron labels are one sufficiently large representative shell; after the canonical stellar-label shift, the incidence pattern is independent of the shell radius. For a seam state s_i, the columns record the coherent source coefficient $144q_i$, the cell potential $144U_i$, the radial degrees (d_-, d_+), the attachments to the two long paths P^+ and P^-, and the seam states joined radially from the previous and to the next shell. Thus the table is an exact certificate for the finite equations

$$L_\Sigma U = q_\Sigma, \qquad 144U_i \in \{0, 1, 2, 3, 4\},$$

and, together with the oriented radial-edge convention in the main text, for the seam-flux identity

$$J_\Sigma = -\frac{1}{18}.$$

The table is included as data rather than as part of the conceptual argument: all later analytic estimates use only the finite consequences stated in the main text.

i	tetrahedron	$144q_i$	$144U_i$	(d_-, d_+)	P^+	P^-	in-states	out-states
0	02151157	0	1	$(3,1)$	0	0	0,1,2	0
1	09157163	-1	0	$(1,2)$	1	0	1	0,1
2	12157163	0	2	$(2,2)$	0	0	2,8	0,2
3	157161162163	1	4	$(2,0)$	1	0	7,8	-
4	161162163165	0	4	$(1,1)$	0	0	-	-
5	161163164165	1	4	$(2,0)$	0	0	9,10	-
6	163164165168	0	4	$(1,1)$	0	0	13	-
7	163164167168	1	4	$(2,1)$	0	0	12,14	3
8	1163167169	0	3	$(1,2)$	0	0	12	2,3
9	1167169170	-1	3	$(1,1)$	0	0	15	5
10	166167170171	1	4	$(2,1)$	0	1	15,17	5
11	2124166172	0	0	$(2,1)$	0	1	11,16	11
12	1169170173	-1	3	$(1,2)$	0	0	18	7,8
13	170171172174	0	4	$(1,2)$	0	0	17	6
14	170172173174	1	4	$(1,2)$	0	0	18	7
15	1172173176	-1	3	$(2,2)$	0	0	18,19	9,10
16	1821172178	0	0	$(2,2)$	0	0	16,20	11,16
17	172176177178	1	4	$(1,3)$	0	0	19	10,13
18	1176178179	-1	3	$(1,3)$	0	0	19	12,14,15
19	1178182184	0	3	$(1,3)$	0	0	21	15,17,18
20	1518178184	0	0	$(2,2)$	0	0	20,22	16,20
21	12184190	0	2	$(2,2)$	0	0	21,23	19,21
22	1215184190	0	0	$(2,2)$	0	0	22,24	20,22
23	02190196	0	1	$(2,2)$	0	0	23,25	21,23
24	912190196	0	0	$(2,2)$	0	0	24,25	22,24

i	tetrahedron	$144q_i$	$144U_i$	(d_-, d_+)	P^+	P^-	in-states	out-states
25	09196202	-1	0	$(1, 3)$	0	0	25	23,24,25

C Exact 32–state first-order corrector certificate

The first-order parametrix of Section 5.4 enlarges the 26 seam states by the six path states at which the coefficient of r^{-1} in $LP_0 - q$ may be nonzero. The following finite certificate records the state ordering, the quotient graph, a nonzero principal cofactor of its Laplacian, and the complete first-order defect vector. In particular it verifies algebraically that

$$\ker \widehat{L} = \mathbb{R}1, \qquad \langle a, 1 \rangle = 0,$$

so that

$$\widehat{L}W = -a, \qquad \langle W, 1 \rangle = 0$$

has a unique solution.

Use the state ordering

$$(s_0, s_1, \ldots, s_{25}, p_0^+, p_{-2}^+, p_{-1}^+, p_0^-, p_1^-, p_{-1}^-).$$

Here $p_0^+ = v_0^+$, $p_{-2}^+ = v_{2r-11}^+$, $p_{-1}^+ = v_{2r-10}^+$, $p_0^- = v_0^-$, $p_1^- = v_1^-$, and $p_{-1}^- = v_{2r-11}^-$. All edges below have multiplicity one. The edge set of the quotient graph is

$$\begin{aligned}
&01, 02, 1p_0^+, 2\,8, 34, 37, 38, 3p_{-1}^+, 45, 4p_{-2}^+, 4p_0^-,\\
&56, 59, 5\,10, 67, 6\,13, 6p_{-1}^+, 7\,12, 7\,14, 89, 8\,12, 9\,12, 9\,15,\\
&10\,15, 10\,17, 10p_0^-, 11\,16, 11p_{-1}^-, 12\,18, 13\,14, 13\,17,\\
&14\,18, 14p_0^-, 15\,18, 15\,19, 16\,20, 17\,19, 17p_1^-, 18\,19,\\
&19\,21, 20\,22, 21\,23, 22\,24, 23\,25, 24\,25, p_{-2}^+p_{-1}^+, p_0^-p_1^-.
\end{aligned}$$

Here, for example, 01 means the edge s_0s_1 and $10p_0^-$ means $s_{10}p_0^-$. This graph is visibly connected, hence its graph Laplacian $\widehat{L}$ has kernel R1. In the displayed ordering, the principal cofactor obtained by deleting the last row and column is

$$\det \widehat{L}^{(32)} = 71\,987\,392.$$

Let B and λ be as in the continuum profile. The coefficient a in

$$LP_0 - q = \frac{a}{r} + O(r^{-2})$$

is, in the same ordering,

$$a = (2\lambda, -\lambda, 0, 2B + 6\lambda, \tfrac{11}{5}B + \tfrac{22}{5}\lambda, 2\lambda, 2B + 4\lambda, \lambda, -\lambda, 0, \lambda, -11B + \lambda,$$

$$-\lambda, \tfrac{2}{5}B - \tfrac{1}{5}\lambda, -\lambda, 0, 0, \tfrac{1}{5}B - \tfrac{8}{5}\lambda, -2\lambda, -2\lambda, 0, 0, 0, 0, 0, -2\lambda,$$
$$-B, -\tfrac{9}{5}B - \tfrac{18}{5}\lambda, -\tfrac{17}{5}B - \tfrac{34}{5}\lambda, \tfrac{1}{5}B + \tfrac{2}{5}\lambda, \tfrac{1}{5}B + \tfrac{2}{5}\lambda, 10B).$$

Direct addition gives

$$\langle a, 1\rangle = 0$$

identically, separately in B and λ. Thus $\widehat{L}W = -a$ has a solution, unique after the normalization $\langle W, 1\rangle = 0$.

Directional incidence of the six added path states

For reproducibility of the expansion producing a, here is the full radial/same-shell neighbor data of the six added states in the reference period $r = 30$. The labels s_i refer to the seam ordering of Appendix B; "in", "same", and "out" mean shells $r-1, r, r+1$. All later periods are obtained by adding 6 to every recent stellar label.

state	tetrahedron	in	same shell	out
p_0^+	9 12 157 163	9 12 151 157	s_1; 12 15 157 163	9 12 163 169
p_{-2}^+	156 157 159 163	s_4	153 156 157 163; 157 159 162 163	156 159 163 169
p_{-1}^+	157 159 162 163	s_6	156 157 159 163; s_3	159 162 163 169
p_0^-	166 167 168 171	s_{14}	166 168 171 172; s_{10}	s_4
p_1^-	166 168 171 172	s_{17}	166 167 168 171; 165 166 168 172	168 171 172 178
p_{-1}^-	24 27 166 172	24 27 160 166	s_{11}; 27 30 166 172	24 27 172 178

This table, together with the undirected quotient edge list above and the Taylor expansions in Lemma 5.3, determines every entry of the first-order defect vector a without an implicit incidence convention.

References

[1] J. W. Alexander, *The combinatorial theory of complexes*, Ann. of Math. (2) **31** (1930), no. 2, 292–320. DOI: 10.2307/1968099.

[2] E. H. Brown, Jr., *Twisted tensor products. I*, Ann. of Math. (2) **69** (1959), no. 1, 223–246.

[3] R. Courant, K. Friedrichs, and H. Lewy, *Über die partiellen Differenzengleichungen der mathematischen Physik*, Math. Ann. **100** (1928), 32–74.

[4] T. Coulhon and L. Saloff-Coste, *Vari'et'es riemanniennes isom'etriques à l'infini*, Rev. Mat. Iberoam. **11** (1995), no. 3, 687–726. DOI: 10.4171/RMI/190.

[5] M. Kanai, *Rough isometries, and combinatorial approximations of geometries of non-compact Riemannian manifolds*, J. Math. Soc. Japan **37** (1985), no. 3, 391–413. DOI: 10.2969/jmsj/03730391.

[6] T. Delmotte, *Parabolic Harnack inequality and estimates of Markov chains on graphs*, Rev. Mat. Iberoam. **15** (1999), no. 1, 181–232. DOI: 10.4171/RMI/254.

[7] R. Frigerio and M. Moraschini, *Gromov's theory of multicomplexes with applications to bounded cohomology and simplicial volume*, Mem. Amer. Math. Soc. **283** (2023), no. 1402, 1–153. DOI: 10.1090/memo/1402.

[8] M. Gromov, *Volume and bounded cohomology*, Publ. Math. IHÉS **56** (1982), 5–99.

[9] G. Hirsch, *Sur les groupes d'homologie des espaces fibrés*, Bull. Soc. Math. Belgique **6** (1954), 79–96.

[10] N. V. Ivanov, *Foundations of the theory of bounded cohomology* (Russian), Zap. Nauchn. Sem. LOMI **143** (1985), 69–109.

[11] N. V. Ivanov, *Foundations of the theory of bounded cohomology*, J. Soviet Math. **37** (1987), no. 3, 1090–1115. DOI: 10.1007/BF01086634.

[12] N. E. Mnëv, *Combinatorial PL fiber bundles and fragmentation of a fiberwise PL-homeomorphism*, Zap. Nauchn. Sem. POMI **344** (2007), 56–173; English translation: J. Math. Sci. **147** (2007), no. 6, 7155–7217; arXiv:0708.4039.

[13] N. E. Mnëv, *A note on a local combinatorial formula for the Euler class of a PL spherical fiber bundle*, Zap. Nauchn. Sem. POMI **507** (2021), 35–58; arXiv:2109.06143.

[14] M. Skopenkov, *The boundary value problem for discrete analytic functions*, Adv. Math. **240** (2013), 61–87. DOI: 10.1016/j.aim.2013.03.002.